Energy Reports 11 (2024) 3224–3244

Contents lists available at ScienceDirect

Energy Reports

journal homepage: www.elsevier.com/locate/egyr

Research paper

Optimizing smart microgrid performance: Integrating solar generation and static VAR compensator for EV charging impact, emphasizing SCOPE index

Monica P Suresh [a], Yuvaraj T [b], Sudhakar Babu Thanikanti [c,d,*], Nnamdi Nwulu [d]

[a] Department of Electrical and Electronics Engineering, Saveetha Engineering College, Chennai 602105, India
[b] Centre for Computational Modeling, Chennai Institute of Technology, Chennai 600069, India
[c] Department of Electrical and Electronics Engineering, Chaitanya Bharathi Institute of Technology, Hyderabad 500075, India
[d] Centre for Cyber Physical food, Energy and Water Systems, University of Johannesburg, Johannesburg 2006, South Africa

ARTICLE INFO

Keywords:
Electric Vehicle
Electric Vehicle Charging Station
Solar Based Distributed Generation
Battery Energy Storage System
Distribution Static VAR Compensator
SCOPE
Improved Bald Eagle Search Algorithm
Smart Microgrid
Radial Distribution Network

ABSTRACT

The rapid global increase in electric vehicle (EV) usage, driven by its low CO_2 emissions, uncomplicated maintenance, and minimal operating costs, has prompted extensive research in the field of electric vehicle charging station (EVCS). The integration of EVCS into the current distribution grid poses challenges due to potential power losses and voltage variations beyond acceptable limits. This complexity is heightened by the growing penetration of randomly dispersed solar-based distributed generation (SDG) and battery energy storage system (BESS). To address these challenges, distribution static VAR compensator (DSVC) systems have been introduced, offering benefits such as enhanced power transfer capacity, improved voltage regulation, and increased system security without requiring extensive infrastructure upgrades. This study offers SCOPE, a novel multi-objective framework that unifies the optimization goals of minimizing real power loss, lowering bus voltage variation, maximizing system voltage stability, minimizing system operating costs, and mitigating CO_2 emissions. The EVCS problem is optimized within this multi-objective framework utilizing an improved bald eagle search algorithm (IBESA). The proposed model accounts for vehicle to grid (V2G) capabilities and the actual driving patterns of users over a 24-h horizon. The formulation of a smart microgrid (SMG) structure is based on modifying the standard IEEE 33-bus test radial distribution network (RDN), comprising three interconnected SMGs serving residential, commercial, and industrial users. The optimization approach based on IBESA is utilized to optimize both the siting and capacity of EVCS as well as renewable energy sources (RESs). The findings show that SDG and DSVC are effective at lowering the SCOPE index, highlighting the advantages of the suggested approach.

1. Introduction

1.1. Motivation and incitement

The surge in fossil fuel consumption, particularly in power generation and transportation, intensifies environmental pollution and contributes to global warming (Fazelpour et al., 2014). In response, nations seek sustainable and eco-friendly energy alternatives to mitigate the substantial threat posed by fossil fuels, which account for 42% and 22% of global CO_2 emissions in the electricity/heat and transportation sectors, respectively (Fig. 1) (Arif et al., 2021). The prevalent use of Internal Combustion Engines (ICE) in vehicles exacerbates climate change, making Electric Vehicles (EVs) a cleaner and more resilient alternative with minimal or no CO_2 emissions (Arif et al., 2021).

Many countries are actively promoting EVs coupled with renewable energy sources (RES) to address environmental concerns (Amini et al., 2016). The appeal of EVs lies in their emission-free operation and reliance on clean energy, positioning them as a viable alternative to traditional transportation (Mozafar et al., 2018). Ongoing research trends reflect a growing acceptance of EVs, contributing to reduced greenhouse gas emissions and decreased reliance on fossil fuels (Sovacool and Hirsh, 2009). The automotive industry is undergoing transformation with the escalating adoption of EVs, projected to reach 66 million units by 2040 (BloombergNEF, 2021). This surge is driven by incentives, a growing cost-benefit ratio, and environmental advantages. However, challenges

* Corresponding author at: Department of Electrical and Electronics Engineering, Chaitanya Bharathi Institute of Technology, Hyderabad 500075, India.
E-mail address: sudhakarbabu66@gmail.com (S.B. Thanikanti).

https://doi.org/10.1016/j.egyr.2024.02.050
Received 11 December 2023; Received in revised form 9 February 2024; Accepted 24 February 2024
Available online 7 March 2024

Nomenclature

U_i	The magnitude of the bus voltages for node i
U_{i+1}	The magnitude of the bus voltages for node i+1
I	Division current
$R_{i,i+1}$	Resistance between nodes i and i+1
$X_{i,i+1}$	Reactance between nodes i and i+1
P_{i+1}	Real power consumption at node i+1
Q_{i+1}	Reactive power consumption at node i+1
$P_{T,loss}$	Total power loss
Nb	Number of buses/branches/nodes
σ	Standard deviation
ρ	Mean value
n_{module}	Number of modules
t_a	Ambient temperature
t_c	Cell temperature
F_{factor}	Fill factor
t_c^{no}	Cell's nominal operating temperature
c_v	Voltage temperature coefficient
c_i	Current temperature coefficient
V_{oc}	Open-circuit voltage
I_{sc}	Short-circuit current
V_{MPPT}	Voltage at the MPPT
I_{MPPT}	Current at the MPPT
φ	Thyristors' firing angle
B_{DSVC}	Equivalent susceptance
B^C	Capacitor reactance
B^L	Inductance reactance
TOC	Total operational cost
MOF	Multi-objective function
CO_2	Carbon dioxide
EV	Electric Vehicle
EVCS	Electric Vehicle Charging Station
SDG	Solar-based distributed generation
BESS	Battery energy storage system
DSVC	Distribution static VAR compensator
IBESA	Improved bald eagle search algorithm
G2V	Grid to Vehicle
V2G	Vehicle to Grid
SMG	Smart microgrid
RDN	Radial distribution network
RES	Renewable energy sources
ICE	Internal combustion engines
FACTS	Flexible Alternating Current Transmission Systems
BFS	Backward Forward Sweep
BIBC	Bus injection to branch current
DNOs	Distribution Network Operators
PSO	Particle Swarm Optimization
GWO	Grey Wolf Optimization
WOA	Whale Optimization Algorithm
DEA	Differential Evolution Algorithm
HHO	Harris Hawks Optimization
MCTLBO	Multi Course Teaching Learning Based Multi objective Optimization
GA	Genetic Algorithm
MPPT	Maximum power point tracking
SOC	State of Charge
VSI	Voltage Stability Index
CVV	Cumulative voltage variation

like high acquisition costs and limited infrastructure, particularly electric vehicle charging stations (EVCSs), hinder widespread adoption (Shaaban et al., 2019). As EVs charge on the electrical grid, radial distribution networks (RDN) face impacts, including increased energy losses and voltage profile degradation (Etezadi-Amoli et al., 2010; Canizes et al., 2019). Despite challenges, the strategic importance of planning EVCSs to meet rising electricity demand is underscored by the benefits of zero emissions and reduced fuel consumption (Alanazi, 2023).

In efforts to combat greenhouse gas emissions and reduce transmission network expansion costs, solar-based RES, such as photovoltaic modules, gain popularity (Gazijahani and Salehi, 2018a). The declining costs of these modules enable widespread deployment, contributing to environmental benefits and optimizing RDN (Krauter, 2018; Khalid, 2020). While traditional power facilities have lower upfront costs,

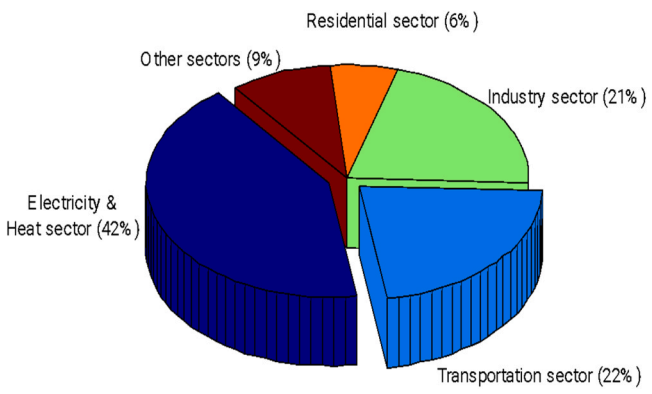

Fig. 1. Sector wise CO_2 emission globally.

combining RES and fossil fuels in large-scale plants offers economic feasibility, improved operating costs, energy flexibility, and system efficiency (Gazijahani and Salehi, 2018b). A comprehensive examination of energy source options is crucial for determining the optimal combination in the RDN. Battery energy storage system (BESS) become critical for RDN optimization, particularly in integrating EVCS, solar-based distributed generation (SDG), and advanced power electronics (Daramola et al., 2023). BESS's rapid energy storage/release and dynamic response to grid dynamics make it pivotal for creating a sustainable, reliable, and efficient power infrastructure. In EV integration, BESS facilitates load management, grid stability, and consistent power supply when paired with SDG. Coordinated with advanced power electronics, BESS contributes to voltage regulation and overall system optimization, playing a key role in the evolving energy landscape.

Within the power electronics industry, flexible alternating current transmission systems (FACTS), including the distribution static VAR compensator (DSVC), revolutionize electricity systems (Rakočević et al., 2021; Abou El-Ela et al., 2020). DSVC enhances power transfer capacity, improves voltage regulation, and boosts system security without extensive infrastructure upgrades. Optimizing DSVC in the RDN involves various indices and techniques (Rakočević et al., 2021; Abou El-Ela et al., 2020). In the context of optimal allocation alongside BESS, EVCS, and SDG, DSVC contributes to mitigating EV and EVCS impacts, aiding in voltage stability. Strategically integrating DSVC within the distribution system holds potential for a more resilient and efficient power infrastructure (Rakočević et al., 2021; Abou El-Ela et al., 2020). Smart microgrids (SMGs) with the proposed optimization achieve the best integration of heterogeneous energy sources in the RDN. SMGs, with self-healing capabilities, seamless RES integration, and demand response support, optimize device allocation for enhanced dependability, resilience, and overall system efficiency. SMGs facilitate optimal

energy management of EVs through active bi-directional communication between utilities and consumers.

1.2. Literature review

Numerous studies have focused on enhancing the strategic planning of EVCS for seamless integration into electrical RDN. Researchers have developed spatiotemporal models to evaluate the impact of different EV charging approaches on the electric grid (Mu et al., 2014). Findings suggest that minimizing losses involves strategically siting EVCS near electrical substations, but challenges arise due to substations' distance from urban areas, leading to increased energy consumption by EVs. Careful consideration of trip expenses and grid losses is crucial in determining EVCS locations. The capacity of EVCS, limited by available land area, poses a challenge requiring thorough investigation (San Román et al., 2011).

Several research articles (Ge et al., 2011; Frade et al., 2010; Li et al., 2011; Hanabusa and Horiguchi, 2011; Jia et al., 2012; Liu et al., 2012a, 2012b; Mohanty and Babu, 2021; Yuvaraj et al., 2023a) have addressed the difficulties of EVCS location and size in the RDN. A partitioning-based strategy, for example, was introduced to optimize EVCS location by minimizing traffic loss (Ge et al., 2011). For the city of Lisbon, optimal EVCS locations with the goal of minimizing station development costs were determined (Frade et al., 2010). The studies established the ideal site of EVCS with an emphasis on decreasing station development costs, and EVCS locations were optimized for EV driving patterns (Li et al., 2011; Hanabusa and Horiguchi, 2011). A graph theory-based study evaluated the ideal location and sizing of EVCS (Jia et al., 2012). Furthermore, developed a two-step strategy that used particle swarm optimization (PSO) to optimize the placement and size of EVCS, with the ideal location identified (Liu et al., 2012a, 2012b). Using the Jaya algorithm (Mohanty and Babu, 2021), the optimal location of EVCS was achieved while accounting for operational expenses, installation costs, and power grid loss. This research explores strategies to alleviate the influence of EVCS on the RDN by optimizing the DG and DSTATCOM, taking into consideration uncertainties in load predictions (Yuvaraj et al., 2023a).

The researcher's utilized PSO optimization considered operating, investment, and maintenance costs, and network constraints (Chen et al., 2019). This research addressed EVCS impact on RDN by exploring modeling and allocation strategies for hydrogen fuel cell-based distributed generation (DG), including a reliability analysis (Yuvaraj et al., 2023a). It determined optimal EVCS positioning in IEEE-33 bus RDN, considering uncertainties in EV numbers (Pal et al., 2019). Placement challenges are tackled using grey wolf optimization/whale optimization algorithm (GWO/WOA) with 2 m point estimate method (2 m PEM) for EV uncertainties, and optimization is done with DE and HHO algorithms (Pal et al., 2021). Implementing distribution static synchronous compensator (DSTATCOM), the study optimizes EVCS configuration in real-time Indian RDNs to reduce power loss (Yuvaraj et al., 2023b). Proposing EV parking lots and DGs positioning in RDN, it employs PSO to choose suitable locations considering economic objectives (Sriabisha and Yuvaraj, 2023). For IEEE-33 and 69 bus RDNs with RESs and BESS-powered EVCSs, the focus is on improving bus voltage, mitigating power loss, and increasing loading capacities (Yuvaraj et al., 2023c). An energy management system optimizes PV/BESS system size and EVCS locations using the multi-course teaching-learning-based multi-objective optimization (MCTLBO) method to reduce annual EVCS operating expenses and system active power loss.

Further, the study investigated optimal EVCS planning in the presence of capacitors within a RDN (Bilal and Rizwan, 2021). Within a traffic-constrained framework, optimal EVCS planning was accomplished (Wang et al., 2013). Achieving optimal EVCS planning within a traffic-constrained framework, the study focused on assessing public sector policies' impact on EVCS expansion, evaluating grid loss and EVCS building costs using genetic algorithm (GA) for EVCS size and placement optimization (Sadeghi-Barzani et al., 2014). Another work modified PSO to achieve optimal EVCS planning, considering building and maintenance costs (Phonrattanasak and Leeprechanon, 2012). EVCS placement within the traffic network, accounting for installation expenses, was addressed in related studies (Simorgh et al., 2018), and cost functions were developed for optimized EVCS deployment considering traffic and geographical limits (Deb et al., 2017). Efficient reduction of power losses was demonstrated in a study optimizing DG sizing and EVCS location within an IEEE 33-bus RDN (Jamian et al., 2014). An intelligent algorithm-based technique addressed EVCS planning challenges, assessing the influence on grid reliability by computing charging cost losses at each location (Bilal and Rizwan, 2023). This study extended the Adaptive PSO method for fast-charging EVCS, incorporating randomly positioned SDG (Ahmad and Bilal, 2023).

1.3. Contribution and paper organization

To the best of the author's knowledge, there has been a substantial amount of research dedicated to the placement and sizing of EVCS inside distribution and transportation networks. However, only a few researchers have looked into this issue while using dynamic load data. Furthermore, the impact of EVCS on voltage and stability inside the distribution grid has not been studied previously using the use of DSVC. Existing studies typically address objectives such as power loss mitigation, voltage profile and stability improvement, operational cost reduction, and CO_2 emission reduction, either separately or in combination. Moreover, most investigations have focused on scenarios involving constant loads within traditional distribution grids. This research uniquely centers on the optimal planning of SDG and DSVC to alleviate the impact of EVCS. The conventional IEEE 33-bus RDN is transformed into a SMG to assess algorithm performance using mixed load models. The study employs an IBESA-based optimization approach to tackle the proposed allocation problem. Additionally, for the first time in an SMG context, the research introduces the use of the SCOPE algorithm for MOF optimization.

The proposed work significantly contributes by addressing critical gaps in the existing literature and overcoming drawbacks associated with previous approaches. The contributions align with specific drawbacks and gaps, strategically filling these voids:

- ***Novel DSVC Integration:*** Introduces a novel integration of DSVC with SDG in the RDN to minimize the impact of EVCS.
- ***Simultaneous Optimization:*** Determines optimal location and capacity of SDG, EVCS, storage facilities, and DSVC concurrently considering uncertainties.
- ***Innovative Conceptual Model:*** Creates a model combining SDG and EVCS to simultaneously mitigate pollutant emissions from power generation and transportation sectors.
- ***Comprehensive Planning with SCOPE Index:*** Conducts optimal planning using a novel SCOPE index, assessing the impact of EVCS load on the SMG in terms of power loss, voltage profile, cost, CO_2 emissions, and stability.
- ***SMG Modification and Evaluation:*** Modifies the IEEE 33-bus RDN as SMG technology and evaluates the proposed approach's efficacy under diverse circumstances.
- ***IBESA Optimization Method:*** Proposes the IBESA method for optimally placing devices in the RDN, ensuring a minimum value of MOF without affecting other parameters.
- ***Dynamic Load Conditions:*** Simultaneously addresses the optimal allocation and sizing of SDGs and DSVCs with EVCSs in the RDN under dynamic loading conditions.
- ***Enhanced EVCS Placement Approach:*** Develops an enhanced approach for optimally placing solar-based EVCS with V2G and G2V facilities.

- ***Optimal Allocation under Mixed Loading Conditions:*** Solves the optimal allocation problem under mixed loading conditions (Residential, commercial, and industrial) in the SMG.
- ***Incorporation of RES and Dynamic Load Levels:*** Addresses the gap in literature by incorporating RES and accounting for dynamic load levels, providing a more realistic representation of the energy system compared to a focus on single load levels.

The subsequent sections of this study are organized as follows: Section 2 outlines the methodology details for the proposed framework. Section 3 introduces the proposed optimization algorithm designed for solving the allocation problem in the SMG. The Simulation Study, conducted using the standard IEEE 33-bus RDN, is presented in Section 4. The study's main conclusions are summarized in Section 5.

2. Proposed framework

2.1. Formulation of the research problem

As mentioned in reference (Jabari et al., 2020), the Backward/Forward Sweep (BFS) technique has gained widespread acceptance for its effectiveness in performing power flow analysis in RDN. The key characteristics of RDN solutions encompass simplicity, speed, minimal memory requirements for processing, and stable convergence. Fig. 2 illustrates a single-line diagram of an RDN incorporating SDG, DSVC, BESS, and EVCS.

The calculation for the bus voltage at $i+1$ is determined by the equation:

$$U_{i+1} = U_i - I(R_{i,i+1} + jX_{i,i+1}) \tag{1}$$

The magnitudes of the bus voltages for nodes $i+1$ and i are denoted by U_{i+1} and U_i, respectively. The link between nodes i and $i+1$ has a resistance and reactance represented by $R_{i,i+1}$ and $X_{i,i+1}$.

The division current I is determined using Eq. (2).

$$I = [BIBC][i] \tag{2}$$

The term 'BIBC' refers to a matrix that describes how injecting current into a particular bus affects the current flow in the branches connected to it.

$$i_{i+1} = \frac{(P_{i+1} + jQ_{i+1})^*}{U_i} \tag{3}$$

The third equation expresses the actual and reactive power consumption at node $i+1$, labeled as P_{i+1} and Q_{i+1} correspondingly, along with the electrical current injected at node $i+1$, represented as i_{i+1}.

Equations are employed to determine the actual and reactive power losses in a system, as given below.

$$P_{loss}(i, i+1) = \left(\frac{P_{i,i+1}^2 + Q_{i,i+1}^2}{|U_i|^2}\right) R_{i,i+1} \tag{4}$$

$$Q_{loss}(i, i+1) = \left(\frac{P_{i,i+1}^2 + Q_{i,i+1}^2}{|U_i|^2}\right) X_{i,i+1} \tag{5}$$

Eqs. (4) and (5) represent the transfer of real power and reactive power between nodes i and $i+1$, respectively. The variables $P_{i,i+1}$ & $Q_{i,i+1}$ represent these power losses. As a result, the sum of branch power losses offers a complete estimate of the system's total losses (6).

$$P_{T,loss} = \sum_{i=1}^{N_b} P_{Loss}(i, i+1) \tag{6}$$

In the above equation, N_b represents the number of branches/nodes/buses.

2.2. Formulation of an EV user load profile

This section outlines the method proposed for constructing a load profile for EVs, which takes into account EV travel patterns, the placement of EVCS, and the charging habits of drivers for various sections such as residential, commercial and industrial area SMGs. The detailed model incorporating these factors is presented below.

2.2.1. Calculation of cumulative load

The cumulative load of EVs can be calculated by considering two main factors: the distance traveled by the EVs and the energy required to cover each kilometer (km). The average daily distance traveled by vehicles typically ranges between 40 and 50 km, with studies indicating that approximately 63% of vehicles cover less than 50 km per day (Darabi and Ferdowsi, 2012; Jaramillo et al., 2009). Additionally, different types of EVs, such as compact sedans, mid-size sedans, mid-size SUVs, and full-size SUVs, exhibit varying energy consumption per km (Kamruzzaman and Benidris, 2018).

To calculate the cumulative load of EVs, we can use the following approach:

$$P_{EV}^{cl} = \sum_{t=1}^{24} \sum_{i=1}^{n_{EV}} \left[d_{EV}^{i} * E_{EV}^{avg,i}\right](i,t) \tag{7}$$

Where P_{EV}^{cl} is the cumulative load, n_{EV} is the total number of EVs, d_{EV}^{n} is

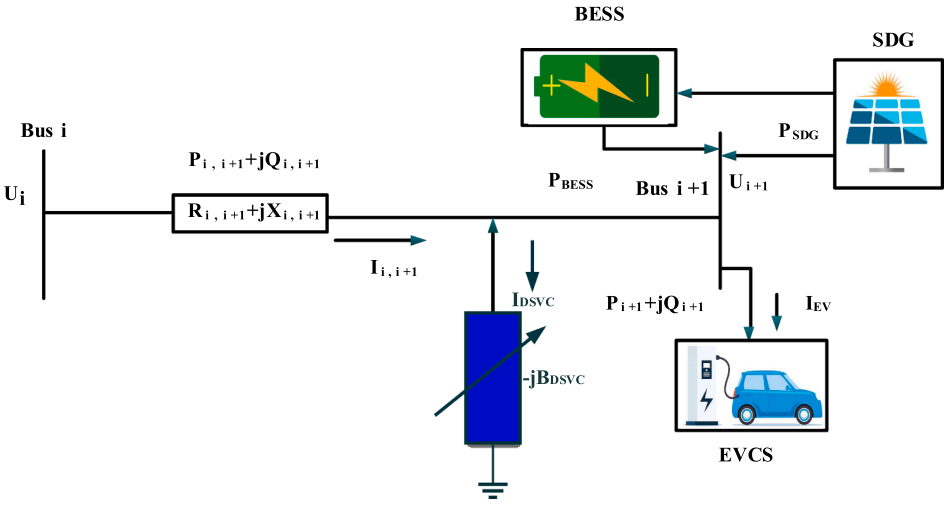

Fig. 2. Single line diagram of RDN with SDG, DSVC, BESS and EVCS.

the average daily distance traveled in km by the i^{th} node EV, and E_{EV}^{avg} is the average energy required to travel each km by the i^{th} node EV.

2.2.2. Bus load

In order to establish a load profile for EVs user at each bus/node, it is necessary to analyze the impacts of the locations of EVCSs and drivers' preferences on the change in demand at system buses. The major percentage of in-home (residential area) charging happens during the off-peak periods whereas public charging stations (commercial/industry areas) are mostly used during peak periods (Kamruzzaman and Benidris, 2018). Therefore, to construct a load profile for EVs at each bus, it is necessary to determine the charging patterns of in-home and public stations at the corresponding bus. For the simplicity, in this research, it is assumed that each SMG is having a EVCSs. Based on this, the load of a bus can be calculated as follows for various load models for various nodes. Bus load for SMG charging stations:

$$\mathrm{P}_{EV}^{Total}(i,t) = P_{\mathrm{int}}^{load}(i,t) + f_{EV}^{load}(i,t) * P_{EV}^{cl} \tag{8}$$

where N_b is the total number of buses that contain EVCSs, $P_{\mathrm{int}}^{load}(i,t)$ is the initial load of i^{th} bus at t^{th} period, $f_{EV}^{load}(i,t)$ is the fraction of total EVs charging load contains i^{th} bus at t^{th} period, and $\mathrm{P}_{EV}^{Total}$is the total load of i^{th} bus at t^{th} period after including the load demand at EVCS.

2.2.3. Load profiles for bus considering movement of EVs user

The EV charging pattern varies based on the type of charging station. Public charging stations saw the majority of activity between 9:00 am to 7:00 pm, while in-home charging stations experienced most charging between 7:00 pm and 3:00 am (Kamruzzaman and Benidris, 2018). Due to EV movement uncertainty, some in-home charging loads (both peak and off-peak) may shift to public stations or vice versa. Moreover, there's a possibility of shifting charging loads between off-peak and peak hours. Accounting for these factors, the bus load profile is constructed as follows.

$$P_{(i+1,t)} = P_{(i+1,t)}^{O} + \left[f_{EV}^{total}(i+1,t) - \sum_{\substack{t_1=1 \\ t_1 \neq t}}^{24} f_{EV}^{load}(i+1,t_1) + \sum_{\substack{m=1 \\ m \neq t}}^{24} m_{EV}^{load}(m,t) - \sum_{\substack{l=1 \\ l \neq t}}^{N_b} f_{EV}^{load}(l,t) + \sum_{\substack{l=1 \\ l \neq t}}^{N_b} m_{EV}^{load}(l,t) \right] P_{EV}^{cl} \tag{9}$$

where, $P_{(i+1,t)}^{O}$ is the total load of the $i{+}1^{th}$ bus without EVs at the t^{th} period, $f_{EV}^{total}(i+1,t)$ is the fraction of the total EVs charging load of the $(i{+}1)^{th}$ bus at the t^{th} period without considering EVs movement, $f_{EV}^{load}(i+1,t_1)$ is the fraction of shifted EVs charging load from the t^{th} period to other periods of the $(i{+}1)^{th}$ bus for hour t_1, $m_{EV}^{load}(m,t)$ is the fraction of shifted EVs charging load to the t^{th} period from other periods of the $(i{+}1)^{th}$ bus, $f_{EV}^{load}(l,t)$ is the fraction of shifted EVs charging load from the ith period of the $(i{+}1)^{th}$ bus to other buses, $m_{EV}^{load}(l,t)$ is the fraction of shifted EVs charging load to the l^{th} bus at the t^{th} period from other buses, and $P_{(i+1,t)}$ is the final load of the $(i{+}1)^{th}$ bus at the t^{th} period with EVs charging loads considering EVs movement.

2.3. Modeling of devices

Concerning the anticipated growth in future energy demand and the escalating concerns about greenhouse gas emissions, addressing the prevention of early earth heating has become a pivotal aspect in the energy management of SMGs. Consequently, substantial investments are being directed towards the adoption of EVs and the replacement of distributed low-scale RESs in lieu of traditional large-scale power plants. Simultaneously, the rapid proliferation of EVs within SMGs, coupled with power quality issues such as network instability and suboptimal bus voltage, underscores the increasing need for employing FACTS based DSVC and developing systematic plans for coordinating the scheduling of EVCS. Furthermore, in light of the aforementioned challenges, addressing and managing the uncertainties arising from RESs' generation pose another significant hurdle for Distribution Network Operators (DNOs). SMGs, facilitated by bidirectional communication between DNOs and consumers, offer precise real-time monitoring of system operations. DNOs can encourage users to shift unneeded consumption from peak to off-peak times by presenting various incentive plans based on this technology and accurate monitoring. This approach improves not just the load profile and procurement costs for DNOs, but also the profitability of EV owners and the overall network reliability. This study focuses on the best way to plan SDG, DSVC, BESS, and EVCS. A concise discussion on the modeling aspects of SDG, DSVC, BESS, and EVCS is provided below.

2.3.1. Model of SDG

The beta Probability Density Function (PDF) serves as the model for solar irradiance during each hour of the day, derived from historical data (Teng et al., 2012). The formulation of the PDF for solar irradiance in each time period (in this study, 1 h) is detailed in (Hung et al., 2014):

$$F(x) = \begin{cases} \dfrac{\Gamma(a+b)}{\Gamma(a)+\Gamma(b)} x^{(\alpha-1)} * (1-x)^{(\beta-1)} & 0 \le x \le 1, a, b \ge 0 \\ 0 Otherwise \end{cases} \tag{10}$$

Eqs. (8) and (9) specify the parameters 'a' and 'b' in detail:

$$a = \frac{(\rho * b)}{(1-\rho)} \tag{11}$$

$$b = (1-\rho)\left(\frac{\rho(1-\rho)}{\sigma^2} - 1\right) \tag{12}$$

Here, σ and ρ represent the standard deviation and mean, respectively. The probability (x) of the solar irradiance state during any given hour can be formulated as:

$$P_D(Z) = \int_{x_1}^{x_2} F(x) \quad dx \tag{13}$$

The solar PV module's output power can be stated as:

$$P_{SDG}(x) = n_{module} * F_{factor} * V_s * I_s \tag{14}$$

$$F_{factor} = \frac{V_{MPPT} * I_{MPPT}}{V_{oc} * I_{sc}} \tag{15}$$

$$V_s = V_{oc} * c_v * t_c \tag{16}$$

$$I_s = x[I_{sc} * c_i * (t_c - 25)] \tag{17}$$

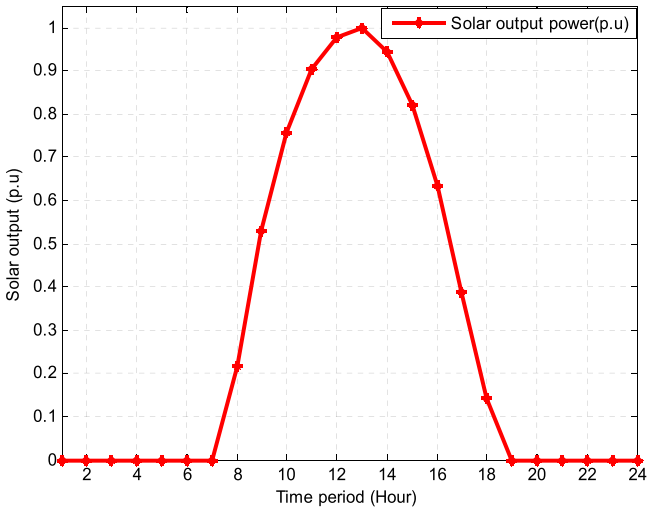

Fig. 3. Solar output load profile.

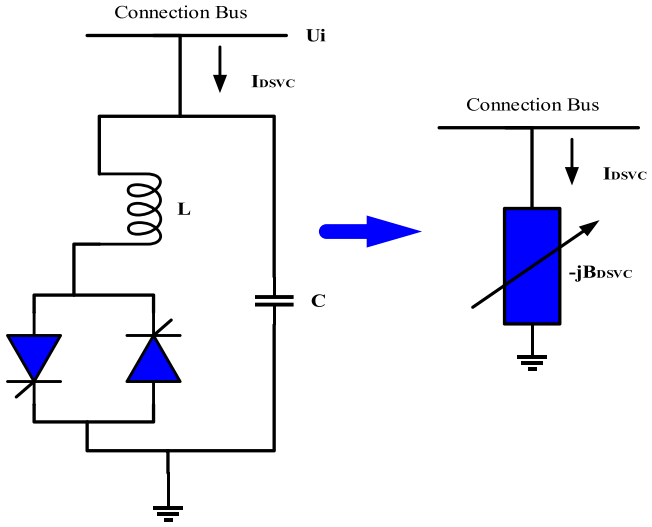

Fig. 4. A model of DSVC device.

$$t_c = t_a + x\left(\frac{t_c^{no} - 20}{0.8}\right) \tag{18}$$

The number of modules is denoted as n_{module}, the ambient and cell temperatures are t_a and t_c, and the current and voltage temperature coefficients are c_i and c_v. t_c^{no}signifies the cell's nominal operating temperature. The fill factor is represented by F_{factor}, and the open-circuit voltage and short-circuit current are represented by V_{oc} and I_{sc}, respectively. The variables V_{MPPT} and I_{MPPT} represent the voltage and current at the maximum power point tracking (MPPT). The entire output power of the PV panel is determined by the specs and irradiance characteristics, which are represented as follows:

$$P_{SDG}(t) = \int_{x_1}^{x_2} P_{SDG}(x) \quad P_D(Z)dx \tag{19}$$

Eq. (19) defines the output power of the solar cell. The solar output load profile, as considered in this study, is depicted in Fig. 3.

2.3.2. Model of DSVC

The basic circuit configuration of a DSVC is depicted in Fig. 4 (Ćalasan et al., 2020). The DSVC consists of a thyristor-controlled reactor running in parallel with a fixed capacitor, illustrating its fundamental components.

The adjustment of the thyristors' firing angle (φ) has a direct impact on the equivalent susceptance of the DSVC, denoted as B_{DSVC}. This correlation can be articulated in the following manner:

$$B_{DSVC} = B^L(\varphi) + B^C \tag{20}$$

$$B^L(\varphi) = -\frac{1}{\omega L}\left[1 - \frac{2\varphi}{\pi}\right] \tag{21}$$

$$B^C = \omega C \tag{22}$$

The relationship governing the equivalent susceptance (B_{DSVC}) is established through the parallel combination of the capacitor reactance (B^C) and the series inductance reactance (B^L). Here, C and L signify the capacitance of the capacitor and the inductance of the reactor, respectively, while U_i represents the voltage magnitude at node i. The reactive power and current controlled by the DSVC device can be described by the following equations:

$$Q_{DSVC} = -B_{DSVC} * U_i^2 \tag{23}$$

$$I_{DSVC} = -B_{DSVC} * U_i \tag{24}$$

When the system load is capacitive, the DSVC absorbs reactive power with thyristor-controlled coils (Q_{DSVC}). When the primary system load is inductive, the DSVC supplies reactive power via parallel-coupled capacitors, improving voltage conditions. The allowable limits of DSVCs are built into the problem, constraining the reactive power function (whether inductive or capacitive).

$$-Q_{DSVC}^{Max} \le Q_{DSVC} \le +Q_{DSVC}^{Max} \tag{25}$$

In the defined equations, $-Q_{DSVC}^{Max}$ and $+Q_{DSVC}^{Max}$represent the limits for injected reactive power, delineating the bounds for inductive and capacitive operation modes of the DSVCs, respectively.

2.3.3. BESS modelling

It is crucial to achieve optimal sizing of the battery to efficiently handle the unpredictable fluctuations in SDG output, aligning it with the varying load demand. A pivotal variable in this context is the SOC, which closely monitors the charging and discharging states of the battery. Overcharging incidents may occur when the hybrid model produces excess power or when the load demand is inadequate. To mitigate this, the control system intervenes by discontinuing the charging process once the battery's State of Charge reaches its maximum value (SOC^{max}). Conversely, to prevent the battery from being depleted, the control system deactivates the load when the SOC hits its minimum value (SOC^{min}) (Geleta et al., 2022). The battery's state of charge undergoes fluctuations based on power output and load demand, playing a pivotal role in the system's energy management. Serving as a dynamic regulator, the battery adjusts power demands and supply. Specifically, when the generated power surpasses the energy requirement, the battery enters a charging state at time *'t'*, as defined by Eq. (26) (Geleta et al., 2022).

$$SOC^{battery}(t+1) = SOC^{battery}(t)(1-\rho) + [P_{SDG}(t) - P_{EVCS}(t)] * \eta^{battery} \tag{26}$$

In instances where RES fall short in generating sufficient power to fulfill the demand, the battery functions as a backup, providing electricity to the load system and operating in a discharging mode. The battery's discharge status at time *'t'* is given as (27):

$$SOC^{battery}(t+1) = SOC^{battery}(t)(1-\rho) + \left[\frac{P_{EVCS}(t) - P_{SDG}(t)}{\eta^{battery}}\right] \tag{27}$$

In the given context, where $SOC^{battery}(t+1)$ and $SOC^{battery}(t)$ represent the state of charge of the battery at time *'t+1'* and *'t'*, respectively, 'ρ' denotes the battery's self-discharge rate, $P_{SDG}(t)$ indicates the power output of the SDG, and battery is the efficiency of the battery's round-trip energy conversion. Eq. (28) can be used to calculate the battery's

round-trip efficiency.

$$\eta^{\text{battery}} = \left(\eta^{\text{battery}}_{\text{charging}} * \eta^{\text{battery}}_{\text{discharging}}\right) \tag{28}$$

In the above scenario, $\eta^{battery}_{charging}$ denotes the battery's charging efficiency, whereas $\eta^{battery}_{discharging}$ denotes the battery's discharging efficiency. The stated round-trip efficiency for the battery bank is 85%. Additionally, it is assumed that the efficiencies for charging and discharging are 90% and 80%, respectively.

$$C_{total} = \frac{SOC^{\max}}{R\text{round} - \text{trip efficiency}} \tag{29}$$

The maximum SOC, denoting the round-trip efficiency of the battery, is associated with the highest SOC value and is equivalent to the overall energy capacity of the battery bank, denoted as C_{total} (in Ampere-hours). This correlation can be expressed as follows (30):

$$\epsilon^{battery}_{total} = \frac{n^{battery}}{n^{battery}_{series}} * \epsilon^{battery}_{single} \tag{30}$$

In this context, $\epsilon^{battery}_{single}$ denotes the energy capacity of an individual battery, while, $n^{battery}$ signifies the total quantity of batteries. Additionally, $n^{battery}_{series}$ indicates the count of batteries interconnected in a series configuration, strategically employed to attain the targeted bus voltage. The discharge of the battery bank is restricted, adhering to a predefined minimal state of charge denoted as $SOC^{\min}$. Depending on the utilization of the battery bank, this constraint may operate as a governing factor within the system.

The formula (31) can be used to calculate the number of batteries arranged in series ($n^{battery}_{series}$):

$$n^{battery}_{series} = \frac{V^{bus}}{V^{battery}} \tag{31}$$

The crucial aspect of battery modeling in this context involves determining the maximum charge/discharge power at any given moment. In the given scenario, where $V^{battery}$ represents the voltage level of an individual battery, and V^{bus} signifies the specific bus voltage of the RDN, this power is influenced by the maximum charging current. The calculation of this power can be expressed using the following Eq. (31):

$$P^{battery}_{\max} = \frac{n^{battery} * V^{battery} * i_{\max}}{1000} \tag{32}$$

In the provided formula, '$i_{\max}$' represents the maximum current for charging, expressed in amperes, while '$P^{battery}_{\max}$' denotes the maximum input/output power capacity of the battery.

2.3.4. EVCS load modeling

A dual converter, charging ports, and EVs are the main components of an EVCS. A regulatory device linked to the charging station enables control of power flow direction at any time. The charging process for EV relies on the SOC of the vehicle, which is characterized as the proportion of the current available charging level to the maximum charging capacity, representing a fully charged battery.Top of Form

SOC offers critical information regarding the battery's required charging level. Several factors influence an EV's power usage, including distance traveled, battery capacity, and driving mode. Eq. (33) can be used to calculate an EV's power consumption.

$$P_{EV} = \frac{d * P_{needed}}{T_{recharge}} \tag{33}$$

In the presented Eq. (33), where d is the distance traveled in km, P_{needed} represents the power required per km, and $T_{recharge}$ indicates the time required to recharge the battery. $SOC^{battery}_{EV}$ is defined by the SOC of the vehicle's battery, which represents the time difference between arrival and departure. The power consumption of an EV can be stated in terms of battery capacity, SOC, and charging time, as shown in Eq. (34).

$$P_{EV} = \frac{C^{battery}_{EV} * (SOC^{\max}_{EV} - SOC^{\min}_{EV})}{T_{recharge}} \tag{34}$$

In the presented Eq. (34), $C^{battery}_{EV}$ represents the EV battery's capacity, while $SOC^{\max}_{EV}$ and $SOC^{\min}_{EV}$ are the maximum and minimum SOC limitations. Consequently, the aggregate power needed to charge a quantity of n_{EV} EVs at a specific time, denoted as t, is expressed as Eq. (35):

$$P^{Total}_{EV} = \sum_{t=1}^{24} \sum_{i=1}^{n_{EV}} P_{EV}(i,t) \tag{35}$$

2.3.5. Operational strategy/ energy management strategies for EVCS

Efficient energy management is critical to ensuring the reliability of any hybrid energy system. The major energy source takes precedence in the specified configuration to exclusively meet the load requirements of the EVCS. The following are the stages for the simplest implementation technique for this energy system. It is assumed in this scenario that the principal energy source is solely responsible for providing the load demand of EVs. Eq. (36) can be used to calculate the difference between the power generated and the power demanded by EVs:

$$\partial P(t) = P_{SDG}(t) - P_{EVCS}(t) \tag{36}$$

When solar panels fall short of satisfying the power requirements for EV loads, more power is obtained from the distribution grid. Furthermore, any excess power generated by the SDG after fulfilling the stated requirements is sold back to the grid.

The simulation will evaluate the following operational ways to apply power management strategies:

- Renewable based SDG serves as the primary source of electricity, delivering sufficient real power to EVCS. Any surplus power is directed to the BESS.
- SDG generates surplus power, meeting overall load requirements, and fully charging the BESS. Excess power beyond the load demands is redirected to a dump load.
- In scenarios where SDG's electrical energy is insufficient for EVCS load requirements, the deficiency is supplemented either by the BESS or the grid, ensuring uninterrupted power supply to EVCS.
- If sustainable energy production is inadequate to meet the required load and the BESS is depleted, the system triggers a resizing process to effectively accommodate energy demands.

2.4. SCOPE index

In power system analyses, there is a lack of indices providing comprehensive insights into the five key operating parameters: stability, voltage, operating cost, power loss, and CO_2 emissions. Stability enhancement is assessed using the VSI (S) value, voltage improvement relies on CVV (C), operating cost is determined by TOC (O), power loss mitigation is evaluated based on real power loss (P) values, and emission reduction is measured using CO_2 emission values (E). To address this gap, a novel index called SCOPE (Voltage Stability, Voltage, Cost, Power Loss, and Emission) is introduced in this study. This index furnishes information on three critical operating parameters of the RDN following any form of disturbance. The SCOPE Index finds application in:

- Optimum charging station position.
- Planning the distribution network with RES.
- Smart microgrid design.
- Distribution network reconfiguration.
- Assessment of network resilience after disturbances.
- Environmental impact analysis.
- Cost-effective operation strategies.

- Integration with smart grid technologies.

2.4.1. Voltage stability (S)

A substantial presence of sensitive and nonlinear loads within the RDN necessitates prompt and significant support in reactive power to ensure the secure and stable operation of the network. Without the provision of reactive power, the RDN may be compelled into an insecure operational state, leading to potential system outages. The vulnerability of the RDN to voltage-related issues may arise if the objective function fails to consider voltage stability. The enhancement of the RDN's security can be notably achieved through the implementation of SDGs and DSVCs. In this context, the assessment of the RDN's Voltage Stability Index (VSI) (Yuvaraj et al., 2020) can be computed using Eq. (37) to evaluate the network's security and stability.

Voltage collapse occurs more frequently on buses with low VSI. VSI measurements can be used to determine the stability of a power supply. If the VSI value is low, an appropriate action can be taken.

$$\mathrm{VSI}(i+1) = |U_{i+1}|^4 - 4\left[P_{i,i+1} * X_{i,i+1} - Q_{i,i+1} * R_{i,i+1}\right]^2 - 4\left[P_{i,i+1} * R_{i,i+1} + Q_{i,i+1} * X_{i,i+1}\right]|U_{i+1}|^2 \quad (37)$$

Approaching a unity value in the VSI signifies enhanced system stability, while nearing zero suggests an unstable operational state for the system. The critical bus, identified as the one associated with the lowest VSI in the RDN, holds particular significance. To evaluate the impact of device allocation on the stability margin, a maximization objective function for system voltage stability (OF_1) is formulated using Eq. (38). This equation represents the ratio of the reciprocal of the VSI for the RDN's critical bus, both with and without considering device allocation.

$$OF_1 = \frac{VSI_a}{VSI_b} \quad (38)$$

OF_1 values may vary, being less than, equal to, or greater than unity. Allocating devices is considered beneficial when the OF_1 value is less than unity. This condition indicates that the VSI of the crucial bus is closer to unity in the presence of devices than in the absence of devices on the RDN.

2.4.2. Bus voltage (C)

Another rationale for allocating SDGs and DSVCs in the RDN is to keep the bus voltage at the load terminals within an acceptable range and to improve the system's voltage profile. Because SDGs and DSVCs can deliver the needed amount of real and reactive into the system while reducing power losses, optimal placement of SDGs and DSVCs into uncompensating systems improves the voltage profile. The network's cumulative voltage variation (CVV) can be expressed as (39):

$$CVV = \begin{cases} 0, \text{if} 0.95 \le U_i \le 1.05 \\ \sum_{i=1}^{N_b} |U_{ref} - U_i|, \text{else} \end{cases} \quad (39)$$

To demonstrate the system's superiority in voltage profile improvement, the CVV at each bus was considered and kept as low as feasible (Thangaraj and Kuppan, 2017). The computations show that the lowest value of CVV represents a significant improvement in the voltage profile of the RDN. By reducing the objective function 2 (OF_2), the voltage profile of the system with SDG and DSVC allocation can be maximized. It is calculated as the ratio of CVV after (CVV_a) and before (CVV_b) system SDG and DSVC placement, and is given by:

$$OF_2 = \frac{CVV_a}{CVV_b} \quad (40)$$

2.4.3. Operating cost (O)

The system's operational costs are divided into two categories. The cost of real electricity delivered by a substation is the primary term. This can be reduced by reducing total power losses in the RDN (Thangaraj and Kuppan, 2017). The cost of real/reactive power provided by the installed SDG and DSVC is the second part. This can be mitigated by reducing the quantity of real/reactive power drawn from SDG and DSVC. Eq. (41) gives the total operational cost (TOC):

$$TOC = (\alpha_1 P_{TL}^a) + (\alpha_2 S_{SDG/DSVC}) \quad (41)$$

Where α_1 and α_2 are the cost coefficients of the substation's and SDG/DSVC's real/reactive power in \$/kW/kVAr. The total real/reactive power drawn from installed SDG/DSVC is denoted as $P_{SDG/DSVC}$. As a result, SDG/DSVC TOC decrease can be stated as:

$$OF_3 = \frac{TOC}{\omega_3 P_a^{max}} \quad (42)$$

OF_3 reflects the system operating cost with SDG/DSVC implemented. By managing OF_3, the operating cost of this system can be decreased.

2.4.4. Power loss (P)

The active power loss is critical in improving the RDN's performance. As a result, the optimal SDG and DSVC placement challenge is primarily focused with minimizing network active power loss. OF_4 is the ratio of total power loss after and before allocation of SDG and DSVC in the RDN, and is given by:

$$OF_4 = \frac{Ploss_a}{Ploss_b} \quad (43)$$

where $Ploss_b$ and $Ploss_a$ are the power losses before and after SDG/DSVC allocation in the RDN Eq. (43) can be used to calculate the system power loss. By lowering OF_4, the total power loss decreased by SDG/DSVC allocation in the RDN can be maximized. An $OF_4$with a value of one indicates that the device allocation has no effect on the RDN's power loss minimization. An OF_4 value less than unity indicates a favorable effect of device allocation. If the OF_4 value exceeds one, it indicates a rise in system power loss when the devices are present, and is therefore deemed an adverse impact on the system.

2.4.5. Emission (E)

The objective function for minimizing CO_2 emissions in a distribution system with SDG, BESS, and EVCS involves calculating CO_2 emissions from grid energy, determining emissions reductions from SDG, BESS, and EVCS. This function aims to optimize the system's components, minimizing the overall carbon footprint by leveraging renewable energy and storage while optimizing EV charging.

$$\mathrm{Emission}(i,t) = E_{factor} * \left[\sum_{i}^{N_b} \times \sum_{t}^{24} \left(P_{grid}(i,t) - P_{SDG}(i,t) - P_{EVCS}^{V2G}(i,t)\right) - P_{BESS}(i,t)\right] \quad (44)$$

where $P_{grid}, P_{SDG}, P_{BESS}$ and P_{EVCS}^{V2G} are variables which denotes the real power delivered by the grid, SDGs, BESS and EVCS (in V2G mode) at bus i and time t, respectively. The corresponding emission per hourly real power generation (TonCo$_2$/MWhr) from the grid is denoted by E_{factor}. They are calculated using 0.910 TonCo$_2$/kWhr (Shaheen et al., 2021).

$$OF_5 = \frac{\mathrm{Emission}_a}{\mathrm{Emission}_b} \quad (45)$$

In this objective function, the goal is to mitigate the total CO_2 emissions by reducing emissions from the grid and maximizing the

contributions of SDG, BESS, and EVCS in emissions reduction. OF_5 is the ratio of CO_2 emissions after and before allocation of SDG and DSVC in the RDN. The CO_2 emissions of this system can be reduced by reducing the OF_5.

2.5. Multi-objective function (MOF)

It has been observed in previous studies that researchers commonly employed different single objective functions in optimizing the allocation problem of SDG/DSVC/EVCS in RDN. However, these objectives often conflict with each other, posing challenges in simultaneously optimizing opposing goals. A multi-objective function comprises a set of functions that need to be optimized concurrently while considering specific operational constraints. Furthermore, optimizing the placement of individual devices and their combinations can greatly improve the performance of the RDN. This optimization can lead to a reduction in power loss, improvement in voltage profile, enhancement of stability margins, reduction in operating costs, and mitigation of CO_2 emissions. Furthermore, in a deregulated system, device owners must gain economic rewards, which incentivizes them to invest in complex equipment. As a result, device allocation must be planned to assure technical and economic benefits. As a result of the foregoing facts, both the technical and economic factors are appropriately merged to develop the MOF as shown in Eq. (46).

$$\begin{aligned}\mathrm{MOF} &= \mathrm{Minimize}(\mathrm{SCOPE}) \\ &= \mathrm{Minimize}\left[\left(\omega_1 * \left(\frac{1}{\mathrm{OF}_1}\right)\right) + (\omega_2 * \mathrm{OF}_2) + (\omega_3 * \mathrm{OF}_3) + (\omega_4 * \mathrm{OF}_4) + (\omega_5 * \mathrm{OF}_5)\right]\end{aligned} \tag{46}$$

The values of the parameters $\omega_1, \omega_2, \omega_3, \omega_4$and ω_5 are adjustable, providing the flexibility to prioritize the impact of specific elements within the overall MOF. The weightage factors are commonly taken as 0.2 for each individual objective functions (OF_1 to OF_5) for the studied method.

2.6. System constraints

The RDN's compensator distribution is established by a set of constraints that includes both equalities and inequalities.

2.6.1. Power distribution

In constructing the power distribution constraints, they can be stated as equalities.

$$P_{T,Loss} + \sum P_{D(i)} + \sum P_{EVCS(i)}^{G2V} = \sum (P_{EVCS(i)}^{V2G} + P_{SDG(i)} + P_{BESS(i)}) \tag{47}$$

$P_{D(i)}$ denotes the power demand at specific buses in the system, $P_{SDG(i)}$, and $P_{BESS(i)}$ denote the power generation from SDG and BESS, respectively, and $P_{EVCS(i)}^{G2V}$ and $P_{EVCS(i)}^{V2G}$ denote the power absorbed (G2V) and supplied (V2G) to SMGs by EVCS, respectively.

2.6.2. Voltage limit

$$U_{i,\min} \le |U_i| \le U_{i,\max} \tag{48}$$

The minimum permitted voltage limit at node i is represented by $U_{i,\min}$, whereas the maximum allowable voltage limit at node i is represented by $U_{i,\max}$.

2.6.3. Reactive power compensation by DSVC

$$\pm Q_{DSVC(i)}^{\min} \le Q_{DSVC(i)} \le \pm Q_{DSVC(i)}^{\max} i = 1, 2, \ldots\ldots\ldots nb \tag{49}$$

The lower and upper limits of reactive power compensation (absorbed/injected) given by the DSVC at bus i are denoted by $Q_{DSVC(i)}^{\min}$ and $Q_{DSVC(i)}^{\max}$, respectively.

2.6.4. Real power compensation by SDG

SDG should inject real power at each optimized bus within the given minimum and maximum limitations.

$$P_{SDG(i)}^{\min} \le P_{SDG(i)} \le P_{SDG(i)}^{\max} i = 1, 2, \ldots\ldots\ldots nb \tag{50}$$

In this case, the lowest real power limits $P_{SDG(m)}^{\min}$ reflect the lower boundaries for the compensated bus i, whilst the maximum real power limits $P_{SDG(m)}^{\max}$ represent the upper bounds for the compensated bus i, which are compensated by SDG.

2.6.5. Real power compensation by BESS

BESS should inject real power into each optimized bus within the prescribed minimum and maximum constraints.

$$P_{BESS(i)}^{\min} \le P_{BESS(i)} \le P_{BESS(i)}^{\max} i = 1, 2, \ldots\ldots\ldots nb \tag{51}$$

The lowest real power limits $P_{BESS(i)}^{\min}$ reflect the lower boundaries for the compensated bus i, while the maximum real power limits $P_{BESS(i)}^{\max}$ represent the upper bounds for the compensated bus i, which are compensated by BESSs.

2.6.6. Line ampacity

The line ampacity constraint can be represented as an inequality constraint in optimization problems. This ensures that the current flowing through the conductor does not exceed its maximum allowable value.

$$I_i \le I_i^{LA,\max} \tag{52}$$

where, $I_{i,t}$ represents the actual current flows in i^{th} line and $I_{i,t}^{LA}$ is the maximum allowable current (ampacity) of the line/conductor in i^{th} line.

2.6.7. Thermal constraint

The thermal constraint for a branch is represented as:

$$S_i \le S_i^{\max} \tag{53}$$

Here, $S_{i,t}$ denotes the apparent power of the node i, while $S_{i,t}^{\max}$ represents the maximum allowable apparent power of the node i. This constraint ensures that the apparent power of the branch does not exceed its maximum allowable value, maintaining the thermal limit of the branch below its upper bound.

3. Proposed optimization algorithm

This section explains IBESA and its importance in defining the ideal placement and sizing of SDG and DSVC to fulfill the goal function inside the IEEE 33-RDN standard. Derived from the original BESA, IBESA takes inspiration from the hunting behavior of bald eagles, specifically during the three crucial sub-processes: space selection, space exploration, and the decisive swooping in on the prey.

3.1. Bald eagle search algorithm

Bald eagles, recognized for their distinctive foraging behavior primarily centered around fish, with a notable emphasis on species like salmon, have inspired innovative meta-heuristic approaches in optimization algorithms. In 2020, H.A. Alsattar et al (Alsattar et al., 2020). introduced the BESA, a novel algorithm that draws inspiration from the hunting strategies of bald eagles, particularly their challenges in capturing fish in water environments. These magnificent birds are capable of hunting from perches as well as using aerial tracking to identify fish from great distances. Bald eagles demonstrate precise flight patterns and smart placement when foraging over bodies of water. These eagles are tough predators at the pinnacle of the food chain, defined as spirits reliant on crucial, protein-rich sustenance. As a result, the BESA

algorithm is divided into three distinct phases, which are discussed further below.

3.1.1. Stage I: selection process

During the first step, the eagle uses the following mathematical expression (54) to locate a probable food source:

$$r_{new,i} = r_{best} + \left[\gamma * \vartheta * (r_{avg} - r_i)\right] \tag{54}$$

The parameter here regulates the degree of position adjustment, which is limited to 1.5–2. The variable ϑ represents a value created at random within the range [0,1]. r_{best} represents the previously determined optimal location, r_{avg} combines data from prior points, r_i represents the current position, and $r_{new,i}$ represents the updated position.

3.1.2. Stage II: search process

During this stage, the eagles navigate inside a preset search zone, executing spirals to increase the intensity of their hunt. The best swoop position is calculated using the following expression (55):

$$r_{new,i} = r_i + q(i) * (r_i - r_{i+1}) + p(i) * (r_i - r_{avg}) \tag{55}$$

$$p(i) = \frac{p\vartheta(i)}{(\max|p\vartheta|)} \tag{56}$$

$$q(i) = \frac{q\vartheta(j)}{(\max|q\vartheta|)} \tag{57}$$

$$p\vartheta(i) = \vartheta(i) * \sin\varphi(i) \tag{58}$$

$$q\vartheta(i) = \vartheta(i) * \cos\varphi(i) \tag{59}$$

$$\varphi(i) = \gamma * \pi * rand \tag{60}$$

$$\vartheta(i) = \varphi(i) + z * rand \tag{61}$$

Eqs. (55) through (61) are implemented during this step of the search. The angle between the location under search and the center point is determined by the parameter, which ranges from 5 to 10. Furthermore, the number of search cycles is determined by the value of z, which ranges from 0.5 to 2. The variable *rand*, which generates values between [0,1], acts as a random number generator.

3.1.3. Stage III: swooping process

In the final stage, all points converge toward the optimal place as eagles swoop towards their objective, mimicking their behavior while grabbing fish from the most promising site. Eq. (62) captures the manifestation of this behavior:

$$r_{new,i} = rand * r_{best} + p1(i) * (r_i - (e_1 * r_{avg})) + q1(i) * (r_i - (e_2 * r_{best})) \tag{62}$$

$$p1(i) = \frac{p\vartheta(i)}{(\max|p\vartheta|)} \tag{63}$$

$$q1(i) = \frac{q\vartheta(j)}{(\max|q\vartheta|)} \tag{64}$$

$$p\vartheta(i) = \vartheta(i) * \sinh\varphi(i) \tag{65}$$

$$q\vartheta(i) = \vartheta(i) * \cosh\varphi(i) \tag{66}$$

$$\varphi(i) = \gamma * \pi * rand \tag{67}$$

$$\vartheta(i) = \varphi(i) \tag{68}$$

In this swooping stage, Eqs. (62) to (68) are also used. The parameters e_1 and e_2 have values between (1 and 2). Furthermore, rand represents a random number between (0 and 1).

3.2. Improved bald eagle search algorithm

In the original BESA, the convergence rate is affected by the use of a fixed controlling parameter γ within the range of 1.5–2 during the search space selection. This fixed parameter can lead to suboptimal performance in terms of both exploration and exploitation. To address this limitation, the IBESA method (Chhabra et al., 2023) introduces an adaptive control parameter. The adaptation allows for dynamic adjustments of the controlling parameter during the optimization process. This adaptability enhances the algorithm's ability to explore diverse regions of the search space effectively, promoting a more robust exploration phase. Simultaneously, it enables the algorithm to exploit promising regions with a finer level of control, leading to improved convergence rates and more accurate identification of optimal solutions. By incorporating adaptability into the controlling parameter, the IBESA method aims to strike a balance between exploration and exploitation, ultimately enhancing the overall efficiency and effectiveness of the optimization process. This adaptability is particularly advantageous in scenarios where the optimal solution may reside in different regions of the search space at different stages of the optimization process.

$$\gamma = 1.5 * \frac{\mathrm{Iter}^{\max} - (\mathrm{i}+1)}{\mathrm{Iter}^{\max}} \tag{69}$$

Where *(i+1)* represents the current iteration count, and $Iter^{max}$ denotes the total number of maximum iterations in the optimization process.

3.3. Procedure for optimization

The IBESA optimization approach for tackling the SDG and DSVC allocation problem is detailed below:

1. ***Initialization:*** Define the number of populations, the number of decision factors (including the quantity, location, and size of SDGs/ DSVCs), and the maximum number of iterations.
2. ***Initial Eagle Search Spaces:*** Randomly initialize eagle search spaces (r_i), estimate the fitness value for each location using Eq. (54), and store the best location.
3. ***Iteration Initialization:*** Set the iteration count (*Iter*) to 1.
4. ***Update Locations:*** Update the locations using Eq. (55) for basic BESA or both Eqs. (69) and (63) for IBESA.
5. ***Evaluate and Update Best Location:*** Evaluate the MOF value for the locations and update the best location found in step 2.
6. ***Further Location Update:*** Update the locations using Eq. (55) and evaluate the MOF value with these new locations.
7. ***Evaluate and Update Best Location (Again):*** Examine the MOF value for the locations received in Step 5 and update the best location discovered in Step 4.
8. ***More Location Updates:*** Update the locations using Eq. (62) and evaluate the MOF value with these new locations.
9. ***Evaluate and Update Best Location (Once More):*** Examine the MOF value for the sites discovered in step 7 and update the best location discovered in step 6.
10. ***Iteration Check:*** If the iteration count (*Iter*) does not exceed the maximum value set, repeat Steps 4–9; otherwise, the optimization process is terminated.

This procedure outlines the sequential steps involved in the IBESA algorithm for addressing the SDG and DSVC allocation problem, incorporating the dynamic updates of search spaces and continuous improvement of the best location throughout the iterations.

4. Simulation study

The research addresses the challenge of optimal allocation of EVCS to effectively manage both active and reactive powers in the presence of

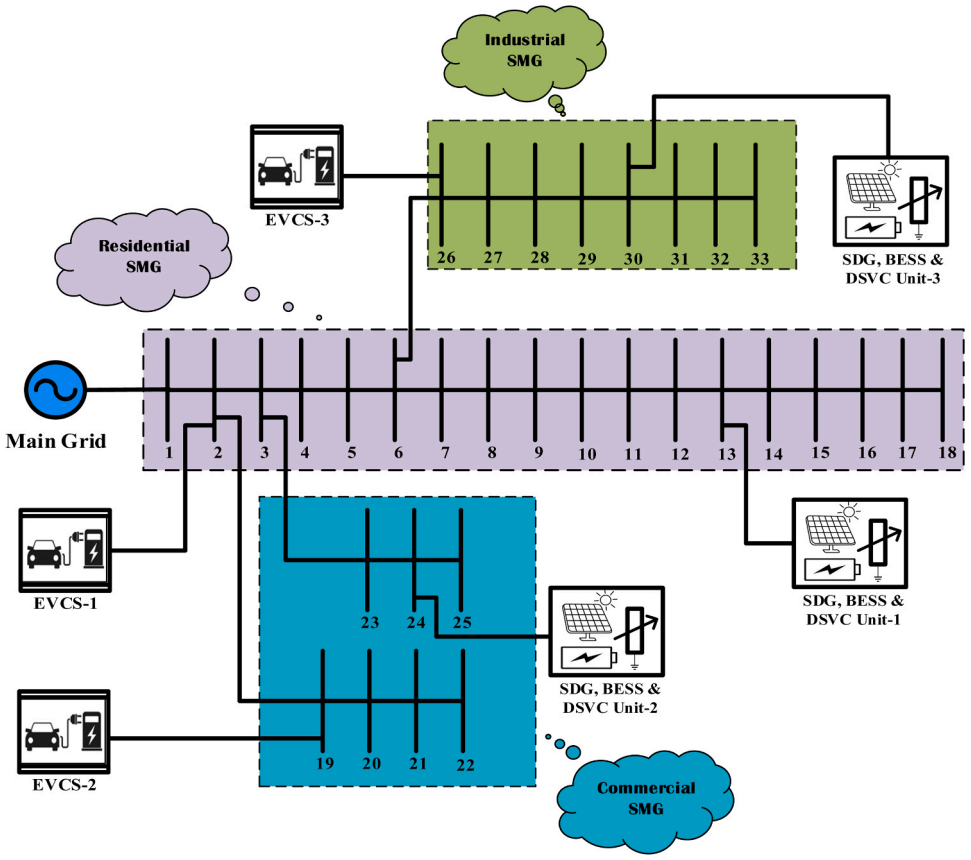

Fig. 5. Modified IEEE 33-Bus System with Three Different SMGs Using Proposed Method.

Table 1
Hourly System Active and Reactive Load Demand (Mixed Load).

Time (Hour)	Load factor	Real Power (kW)	Reactive Power (kVAr)	Time (Hour)	Load factor	Real Power (kW)	Reactive Power (kVAr)
1	0.867	3097.37	1500.66	13	0.911	3254.57	1576.81
2	0.852	3043.79	1474.69	14	0.904	3229.56	1564.7
3	0.837	2990.2	1448.73	15	0.907	3240.28	1569.89
4	0.83	2965.19	1436.61	16	0.911	3254.57	1576.81
5	0.83	2965.19	1436.61	17	0.915	3268.86	1583.74
6	0.859	3068.79	1486.81	18	0.919	3283.15	1590.66
7	0.889	3175.97	1538.73	19	1	3572.52	1730.86
8	0.926	3308.15	1602.78	20	1	3572.52	1730.86
9	0.933	3333.16	1614.89	21	0.963	3440.34	1666.82
10	0.937	3347.45	1621.82	22	0.911	3254.57	1576.81
11	0.941	3361.74	1628.74	23	0.889	3175.97	1538.73
12	0.933	3333.16	1614.89	24	0.867	3097.37	1500.66

various SDG units, including BESS and DSVC. The IEEE 33-bus system serves as the foundation, drawing from Reference (Augugliaro et al., 2010), and incorporates diverse load models outlined in Reference (Kaliaperumal Rukmani et al., 2020). The modified system features an actual power demand of 3.57 MW, a reactive power demand of 1.73 MVAr, and a line voltage of 12.66 kV. The proposed SMG structure, depicted in Fig. 5 based on the modified IEEE 33-bus test system (Shamshirband et al., 2019), comprises three interconnected SMGs catering to residential, commercial, and industrial users. Table 1 provides the details of hourly system active and reactive load demand for a typical day. Each SMG operates independently with distinct hourly active and reactive load profiles, as graphically illustrated in Fig. 6 using daily forecasted load profiles. The loads are combined with various load models (mixed load) such as residential, commercial, and industrial loads Simulations were executed within the MATLAB environment. MATLAB served as a tailored tool for developing a BFS specific to the RDN, enabling the computation of real and reactive power losses and bus voltage values in the absence of any compensation.

The IBESA was used to solve the EVCS allocation problem within the SMG. The study includes 100 EVs (Residential-30EVs, Commercial-15EVs, and Industrial-55EVs) with a 19 kW charging rate, three EVCS with numerous charging stations, and a maximum of one SDG/BESS/DSVC appropriately located in each SMG. The number of EVs in G2V and V2G modes, as well as charge and discharge speeds, determine the EVCS load. The charging rate for G2V mode was 19 kW, whereas the discharge rate for V2G mode was 8 kW (Mohamed et al., 2013). Charging and discharge efficiencies ranged from 80% to 95%, with G2V mode efficiency assumed to be 90% and V2G mode efficiency considered to be 80%. In this study, the EV battery is charged with a power of 15 kW and a battery capacity of 50 kWh. To enhance objective values, a minimum of one compensator (SDG/BESS/DSVC), along with an EVCS in each SMG, is strategically positioned and sized at optimal locations within the

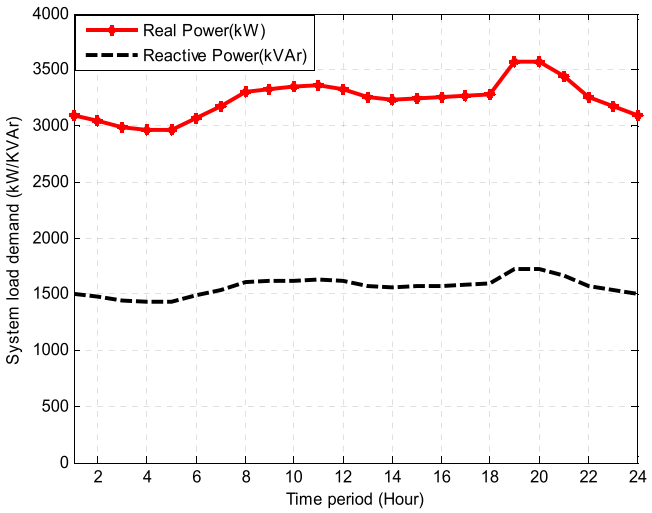

Fig. 6. Hourly System Active and Reactive Load Demand Profiles (Mixed Load).

RDN using the proposed IBESA. SDG, BESS, and DSVC are co-located at the same positions within the SMGs. The size of BESS is determined based on the size of SDG at a specific location within the SMG in the RDN. While DSVC is capable of both injecting and absorbing reactive power in the system, the proposed work only considers injecting reactive power into all three SMGs. This DSVC, installed in the RDN, serves the purpose of enhancing voltage and stability. The decision to limit the DSVC to injecting reactive power, without absorption, is made with the understanding that further improvement is not achieved by allowing both injection and absorption of reactive power, adhering to the specified constraint.

The proposed SMGs-based IEEE 33-RDN test system comprises three distinct regions: residential, commercial, and industrial loads. As a result, the load factor varies among the nodes within the same hour in the simulation. Each SMG in the RDN hosts one SDG and DSVC, optimally placed. Specifically, the optimal locations within SMGs are the 13th node for Residential SMG, the 24th node for Commercial SMG, and the 30th node for Industrial SMG. The load factors for various load models at each node for different hours are detailed in Table 2, sourced from references (Shamshirband et al., 2019). Fig. 7 illustrates the active power load profile under various load models and node locations for the proposed approach. Similarly, the load profile for EV users under different load models is obtained from references (Kamruzzaman and Benidris, 2018; Tran-Quoc et al., 2012). The optimal locations of EVCS within SMGs are identified as the 2nd node for Residential SMG, the 19th node for Commercial SMG, and the 26th node for Industrial SMG. Fig. 8 displays the EV load profile under various load models and locations.

The optimal location and sizing of SDG and DSVC are determined by the proposed IBESA for various load models based on the nodes in the IEEE 33-RDN. Fig. 9 presents a comprehensive flowchart outlining the suggested optimization method using IBESA to find the appropriate location and sizing of SDG and DSVC in the RDN.

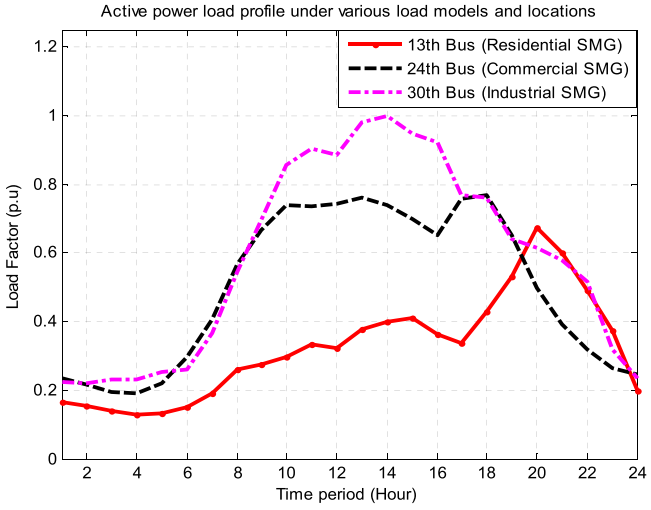

Fig. 7. Active Power Load Profile under Various Load Models and Locations.

Table 2
Hourly SDG and DSVC Real and Reactive Power Outputs under Various Load Factors and Locations (Nodes).

Time (Hour)	13th Location (Residential)			24th Location (Commercial)			30th Location (Industrial)		
	Load Factor	SDG (kW)	DSVC (kVAr)	Load Factor	SDG (kW)	DSVC (kVAr)	Load Factor	SDG (kW)	DSVC (kVAr)
1	0.165	0	38	0.234	0	96	0.225	0	129
2	0.154	0	35	0.217	0	82	0.22	0	127
3	0.142	0	29	0.194	0	85	0.231	0	122
4	0.131	0	28	0.191	0	74	0.231	0	123
5	0.134	0	28	0.22	0	85	0.254	0	135
6	0.151	0	35	0.297	0	119	0.262	0	149
7	0.191	0	42	0.408	0	150	0.368	0	215
8	0.261	39.15	65	0.568	119.85	260	0.546	106.47	304
9	0.277	97.78	65	0.668	350.7	291	0.697	345.02	420
10	0.297	147.91	71	0.74	554.26	361	0.857	634.18	496
11	0.334	210.42	79	0.737	606.55	348	0.905	767.44	550
12	0.322	209.62	76	0.742	717.51	323	0.888	809.86	535
13	0.377	248.82	93	0.762	677.42	321	0.98	894.74	552
14	0.4	253.6	93	0.74	652.68	340	1	850	562
15	0.411	215.78	97	0.7	555.8	284	0.947	714.04	563
16	0.362	151.32	89	0.651	367.16	274	0.922	533.84	519
17	0.337	85.94	92	0.76	277.4	321	0.771	280.64	426
18	0.431	41.38	117	0.771	104.86	305	0.762	101.35	466
19	0.531	0	146	0.651	0	306	0.642	0	398
20	0.674	0	185	0.5	0	235	0.617	0	383
21	0.602	0	158	0.394	0	182	0.58	0	358
22	0.491	0	121	0.32	0	135	0.517	0	291
23	0.374	0	83	0.265	0	98	0.32	0	187
24	0.2	0	46	0.245	0	100	0.237	0	136

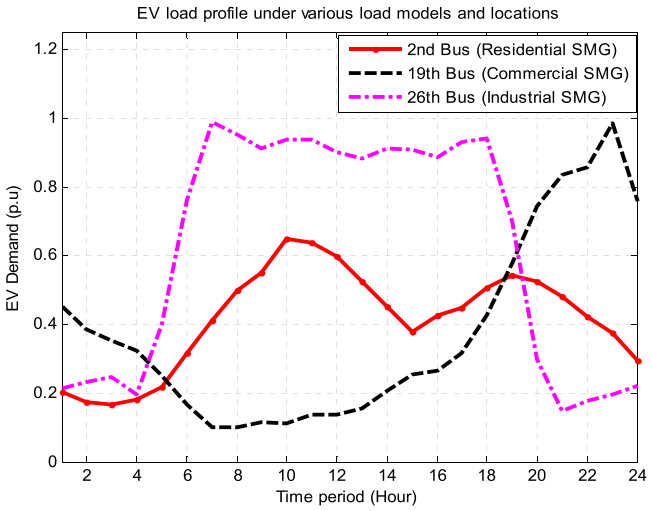

Fig. 8. EV Load Profile under Various Load Models and Locations.

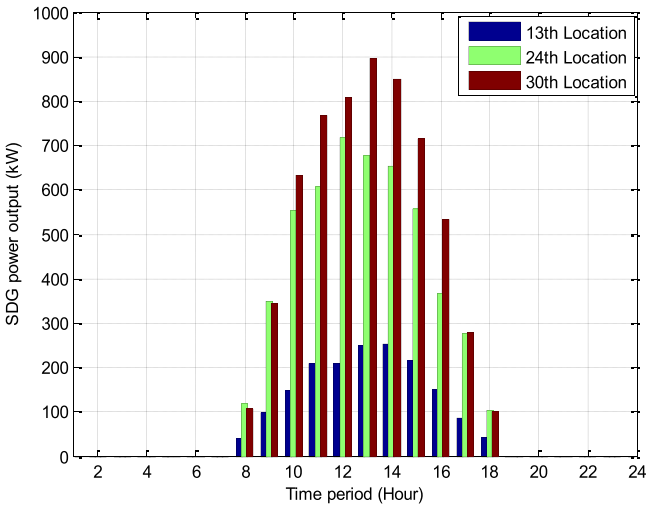

Fig. 10. Hourly SDG Output (kW) under Various Load Factors and Locations.

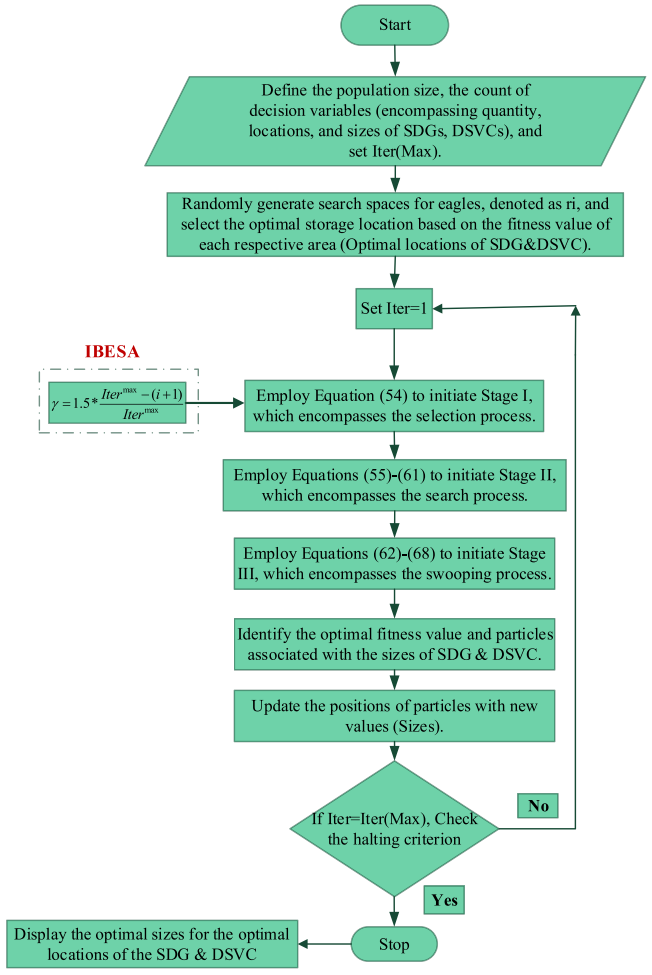

Fig. 9. Implementation Process of the IBESA for the proposed work.

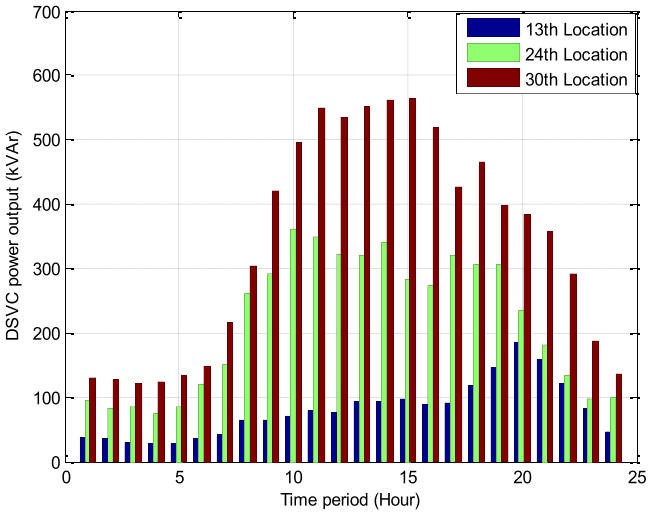

Fig. 11. Hourly DSVC Output (kVAr) under Various Load Factors and Locations.

4.1. Numerical results

This section outlines the novel methodology proposed in this paper for mitigating the impact of EVCS in the RDN while minimizing the SCOPE index. The study also delves into the uncertainties associated with SDG and system load by applying the suggested optimization approach. Utilizing V2G technology and enabling two-way power exchange between EVCSs and SMGs significantly reduces the need to purchase power from the upstream network, thereby reducing dependence on the main grid. The model and optimization problem for SMGs in a 24-h operational time horizon are detailed in this section. This timeframe is chosen to explore the impact of uncertainties in SDG-based units and load consumptions within various scenarios on DSVC units, BESS, and responsive loads. To determine the optimal placement of EVCS on the RDN, an optimal number of EVCS units needs to be deployed at strategic bus locations. Since EVCS installation increases active power loss and affects other parameters of the SCOPE index in the network, SDGs and DSVCs are optimally positioned to compensate for these losses. The IBESA is employed to optimize the SCOPE index. Before integrating EVCS and SDG/DSVC, a BFS approach-based power flow study is conducted to establish baseline losses. The optimal locations and sizes of SDG and DSVC units are presented in Table 2, while the corresponding multipliers for hourly forecasted real and reactive power outputs from SDG and DSVC are depicted in Figs. 10 and 11, respectively. The optimal placement of SDG/DSVC units is identified at the 13th, 24th, and 30th buses within each SMG. BESS units are co-located with SDG units, storing power during periods when EVCS is not actively drawing power and discharging during peak hours to support the SMGs.

In the evolving landscape of future distribution systems, SMGs bear a crucial responsibility in enhancing the technical specifications of RDN by actively providing ancillary services to the network. A fundamental requirement for SMGs is to support the real and reactive demand of the network, aiming to improve key aspects such as voltage stability, operational cost efficiency, power loss reduction, and the mitigation of CO_2 emissions within the system. Figs. 10 and 11 present a comprehensive depiction of the generated real and reactive powers of SDG and DSVC units over a 24-h period with different load factors. This study strategically incorporates EVCSs to elucidate the influence of EVs on the generation patterns of SDGs. By actively participating in the generation of real and reactive powers, SDG units contribute to meeting the real and reactive demand of the network, thereby positively impacting voltage stability and overall system performance. Additionally, DSVC units play a crucial role in providing reactive power support, enhancing voltage regulation, and addressing stability concerns within the system. This integration of SMGs, especially with the inclusion of EVCSs, not only supports the technical requirements of the RDN but also highlights the dynamic interaction between emerging technologies like EVs and the generation capabilities of SDG and DSVC units. Such insights are vital for designing robust and adaptive future distribution systems that can effectively meet the evolving demands of a sustainable and resilient energy landscape.

Table 3 provides a detailed information of the hourly EVCS demand and the corresponding modes of operation. Additionally, Figs. 12 and 13 offer a comprehensive examination of the charging and discharging patterns of both EVCS and BESS over a 24-h period on the RDN under various load factors and locations. Based on the literature study findings, V2G services appear more viable during the middle of the day, while G2V services are more prevalent in the evening. Given the diverse load models in the proposed approach's test system, G2V operations are scheduled from 5 p.m. to 9 p.m. (evening), whereas V2G operations are scheduled from 10 a.m. to 3 p.m. (middle of the day) for the simulation study. This strategic scheduling ensures that EVCSs leverage surplus power generated by the SDG units during their peak performance hours. Conversely, during peak demand periods when grid demand is highest, all three EVCSs seamlessly transition into discharging mode (V2G mode). This mode enables EVs to supply power back to the grid, thereby contributing to grid support and demand management efforts.

Table 3
Hourly EVCS Demand and Modes of Operation under Various Locations (Nodes).

Time (Hour)	EVCS demand (kW)			Modes of operation (G2V/V2G/Ideal)
	2^{nd} Location	19^{th} Location	26^{th} Location	
1	0	0	0	Ideal
2	0	0	0	Ideal
3	0	0	0	Ideal
4	0	0	0	Ideal
5	0	0	0	Ideal
6	0	0	0	Ideal
7	0	0	0	Ideal
8	0	0	0	Ideal
9	0	0	0	Ideal
10	539.76	30.1008	1572.33	V2G
11	534.1027	36.3274	1514.36	V2G
12	494.3378	36.219	1502.02	V2G
13	423.6422	40.4957	1440.4	V2G
14	360.3158	54.439	1473.23	V2G
15	304.3351	65.785	1475.57	V2G
16	0	0	0	Ideal
17	410.7485	93.3667	1715.45	G2V
18	466.4336	125.859	1742.04	G2V
19	544.5121	185.632	1420.01	G2V
20	524.1593	239.604	602.311	G2V
21	468.313	258.516	290.359	G2V
22	0	0	0	Ideal
23	0	0	0	Ideal
24	0	0	0	Ideal

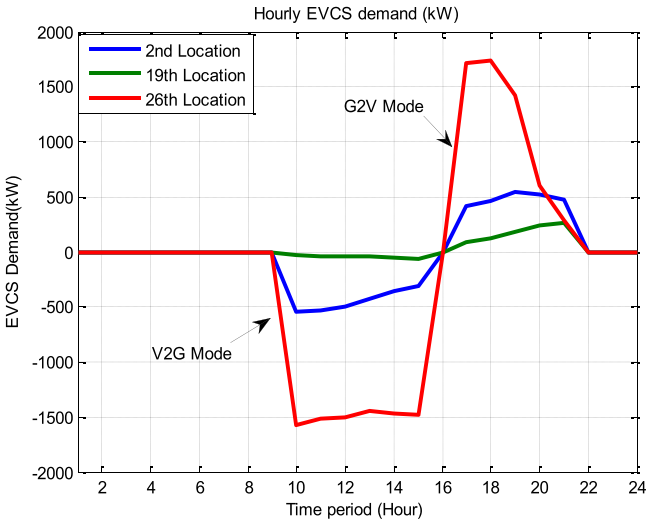

Fig. 12. Hourly EVCS Demand (kW) under Various Load Factors and Locations.

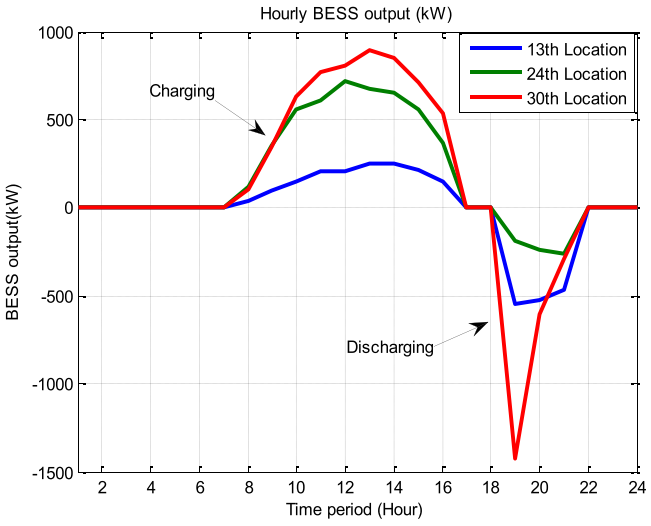

Fig. 13. Hourly BESS Output (kW) under Various Load Factors and Locations.

In scenarios where the power supplied by the SDG units is insufficient to meet the required demand, the EVCSs have the capability to draw additional power from the grid. Notably, during periods when the EVCSs are in an idle state and not actively charging or discharging, any surplus power is stored in the BESS. This stored energy is strategically discharged during peak demand hours, further optimizing the utilization of resources and supporting the grid when additional power is needed. This dynamic operation of EVCSs and BESS, synchronized with the varying patterns of SDG output and grid demand, exemplifies an intelligent and adaptive approach to managing power flows within the RDN. It not only enhances the efficiency of power utilization but also contributes to the overall stability and reliability of the system, aligning with the evolving requirements of modern smart grids.

4.2. Effect of EVCS Load on SCOPE Index

The analysis of the impact of EVCS load on the distribution network's SCOPE index was carried out over a 24-h period, as shown in Table 4. This subsection describes the findings of this investigation, which shed insight on the dynamic relationship between EV charging operations and the overall performance of the RDN.Top of Form

Table 4
Hourly Performance Analysis of SCOPE Index.

Time (Hour)	Load factor	Voltage Stability (p.u)		CVV (p.u)		TOC ($)	Power Loss (kW)		Emission (ton/kWhr)	
		Before	After	Before	After	After	Before	After	Before	After
1	0.867	0.7413	0.7509	0.0706	0.0676	1743.8	116.36	107.2	2818.62	2818.62
2	0.852	0.7456	0.7547	0.0693	0.0665	1634.36	112.15	103.59	2769.85	2769.85
3	0.837	0.7498	0.758	0.068	0.0655	1580.2	108.02	100.05	2721.09	2721.09
4	0.83	0.7518	0.7599	0.0674	0.0649	1518.52	106.13	98.38	2698.33	2698.33
5	0.83	0.7518	0.7603	0.0674	0.0648	1631.12	106.13	97.78	2698.33	2698.33
6	0.859	0.7436	0.7536	0.0699	0.0668	1931.4	114.1	104.1	2792.61	2792.61
7	0.889	0.735	0.7481	0.0725	0.0685	2471.28	122.69	109.07	2890.14	2890.14
8	0.926	0.7245	0.7584	0.0758	0.0652	4856.03	133.77	95.92	3010.43	2768.85
9	0.933	0.7225	0.7866	0.0764	0.0567	8104.34	135.92	64.21	3033.18	2311.1
10	0.937	0.7214	0.8382	0.0767	0.0417	22234.6	137.16	50.47	3046.19	0
11	0.941	0.7203	0.8587	0.0771	0.0359	23402.8	138.41	42.94	3059.19	0
12	0.933	0.7225	0.8633	0.0764	0.0347	23695.8	135.92	44.48	3033.18	0
13	0.911	0.7288	0.8834	0.0745	0.0291	23608	129.21	37.61	2961.66	0
14	0.904	0.7308	0.8846	0.0738	0.0288	23347.8	127.12	37.87	2938.91	0
15	0.907	0.7299	0.8681	0.0741	0.0334	21533.2	128.01	39.16	2948.66	0
16	0.911	0.7288	0.8194	0.0745	0.0471	9845	129.21	43.35	2961.66	2004.05
17	0.915	0.7276	0.7641	0.0748	0.0635	19245.2	130.42	183.13	2974.67	2388.65
18	0.919	0.7265	0.7467	0.0752	0.0688	18240	131.635	222.6	2987.67	2762.36
19	1	0.7037	0.7152	0.0823	0.0786	15971.8	157.55	242.76	3251	3251
20	1	0.7037	0.7305	0.0823	0.0738	11523.7	157.55	169.59	3251	3251
21	0.963	0.7141	0.7409	0.079	0.0706	9134.34	145.39	139.6	3130.71	3130.72
22	0.911	0.7288	0.7543	0.0745	0.0665	3175.68	129.21	110.17	2961.66	2961.66
23	0.889	0.735	0.7523	0.0725	0.0672	2276.88	122.69	109.22	2890.14	2890.14
24	0.867	0.7413	0.7522	0.0706	0.0672	1836.2	116.36	106.55	2818.62	2818.62
Average	**0.905**	**0.7304**	**0.7834**	**0.0739**	**0.0581**	**10605.9**	**127.96**	**102.492**	**2943.65**	**2080.3**

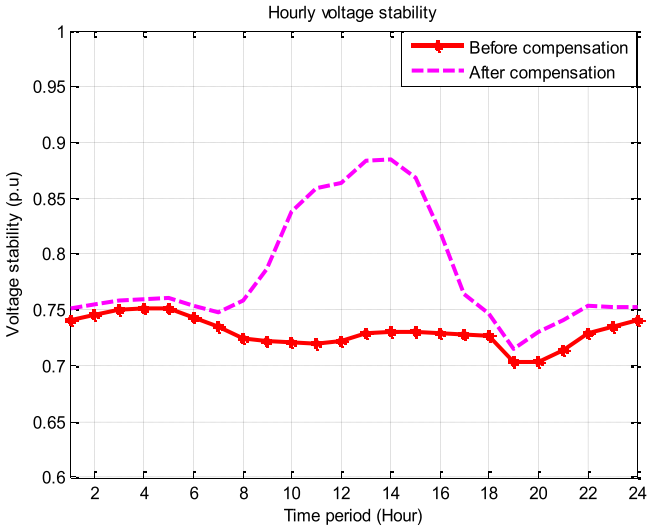

Fig. 14. Hourly Voltage Stability.

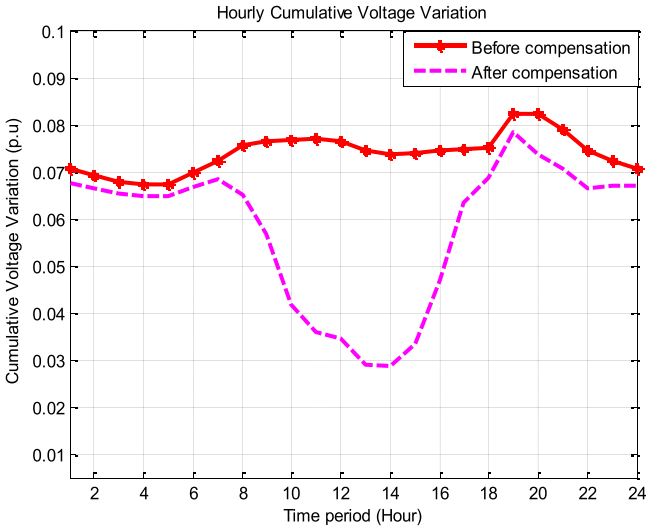

Fig. 15. Hourly Cumulative Voltage Variation.

4.2.1. Effect of EVCS Load on Voltage Stability

This subsection addresses the evaluation of the EV charging load's impact on the voltage stability of the modified IEEE 33-bus test RDN. The VSI is calculated for all buses using the proposed methodology. Table 4 presents the VSI values for the base case (before compensation) and subsequent to the placement of EVCS and other compensators (after compensation). The VSI serves as an indicator of bus stability, with values ranging between 0 and 1. Buses with higher VSI values close to one are considered stable, while those with lower values near zero are deemed prone to instability and require attention. The strategic placement and sizing of EVCSs and SDGs are contingent upon the continuous decline and abrupt rise in VSI. Fig. 14 illustrates the VSI values for the base case, after EVCS placement during charging times, and after considering SDGs and DSVC for a 24-h period. Notably, the installation of EVCS load at robust buses (bus 2, 19, and 26) mitigates the degradation of voltage stability.

Furthermore, the stability index of the system's weakest buses improves with the introduction of SDGs, considering the base values across all load levels throughout the day. The VSI values exhibit improvement for all buses with SDG and DSVC placement compared to EVCS placement alone. Consequently, the likelihood of voltage instability is reduced, rendering the system more stable with the combined deployment of SDGs and DSVCs. This underscores the effectiveness of integrating renewable energy sources and compensating devices in enhancing the voltage stability of the RDN, particularly in the context of EV charging scenarios.

4.2.2. Effect of EVCS load on cumulative voltage variation

Table 4 provides the CVV for all load levels, depicting values for the base case, as well as after the placement of EVCSs, SDG, and DSVC. The CVV serves as an indicator of the voltage profile of the system, with lower values indicating an improved voltage profile. Fig. 15 further

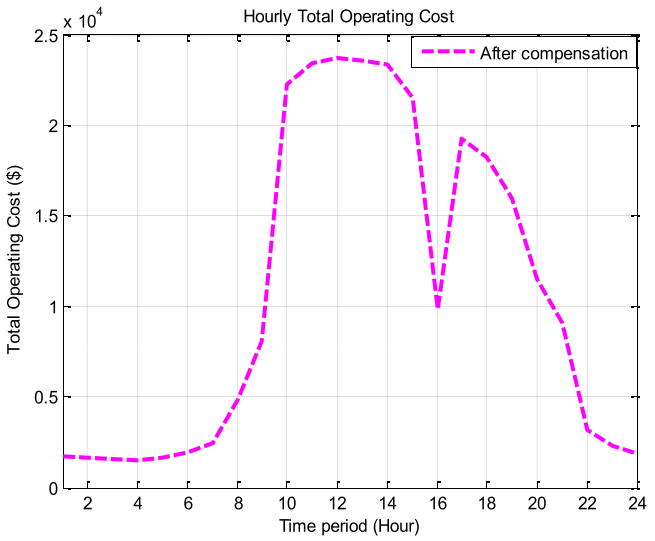

Fig. 16. Hourly Total Operating Cost.

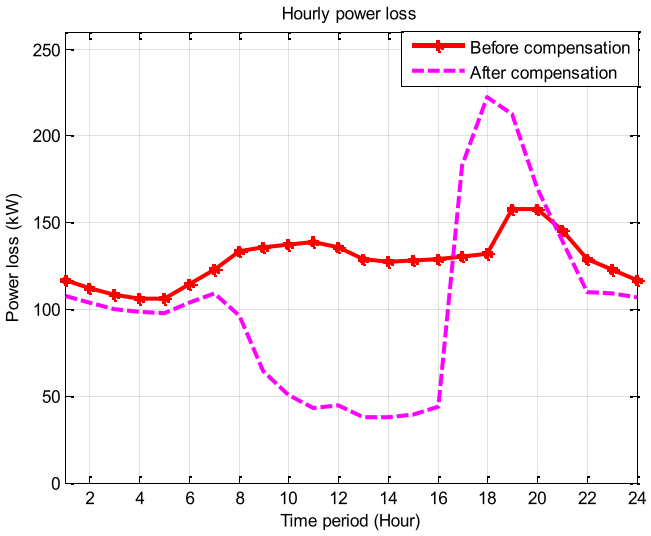

Fig. 17. Hourly power loss.

illustrates the hourly CVV of the modified 33-bus system over a 24-hr period. Notably, the minimum CVV occurs during the hours from 8 a.m to 6 p.m, while the CVV values reach their maximum during the periods from 1 a.m to 7 a.m and 7 p.m to 12 a.m. These variations align with the charging and discharging cycles of EVCSs implemented in the proposed method. The introduction of SDG and DSVC results in significant mitigation of CVV, particularly during the peak demand hours. The peak mitigation is observed after the installation of SDG and DSVC, contributing to a substantial reduction in losses and an overall enhancement of system performance. This analysis underscores the effectiveness of integrating RES and compensating devices, such as SDG and DSVC, in not only improving the voltage profile of the distribution network but also mitigating voltage variations induced by EV charging and discharging activities. The observed reduction in CVV signifies enhanced stability and resilience of the system, showcasing the potential of the proposed methodology to optimize system performance in the presence of EVCSs.

4.2.3. *Effect of EVCS load on total operating cost*

Table 4 outlines the TOC of the proposed method following the installation of compensating devices. The TOC is computed based on power loss values and the corresponding sizes of compensators (kW/kVAr). Fig. 16 graphically represents the Hourly TOC of the proposed approach after the implementation of SDG and DSVC in the modified IEEE-33 RDN. The TOC is influenced by the values of power loss and the sizing of compensators, and its trends provide insights into the economic efficiency of the proposed methodology. The operating cost experiences an increase during G2V mode, reflective of the energy consumption pattern during this phase. Conversely, the operating cost decreases during V2G mode, as EVs contribute power back to the grid. It is crucial to note that despite potential economic losses associated with improper placement of charging stations leading to a higher TOC, the implementation of EVs with a V2G scheme yields a net benefit that cannot be overlooked. The net economic gain derived from the V2G scheme outweighs the drawbacks, emphasizing the overall economic viability and positive impact on the operating cost despite initial challenges associated with EV charging stations. This analysis highlights the importance of strategically managing the operating cost dynamics, considering both charging and discharging modes, to maximize the economic benefits of integrating EVs and compensating devices within the distribution network.

4.2.4. *Effect of EVCS load on power loss*

Mitigating power loss is a crucial objective for network operators, particularly after the installation of EVCS in the RDN. This subsection presents an analysis of the impact of EVCS loads on the power loss of the distribution network over a 24-h period, considering different load factors as outlined in Table 4. Fig. 17 visually represents the magnitude of power loss in the network both before and after the placement of EVCS, SDG, and DSVC. It is evident that improper placement of EVCS and compensating devices leads to higher power losses compared to optimal placement strategies. Post-installation of EVCSs alone, the power loss in the distribution network tends to increase. However, this increased power loss is effectively controlled by strategically placing SDG and DSVC within the RDN. The power loss is minimized when SDG produces maximum power, typically during periods of ample sunlight. Additionally, during peak hours, EVCSs are operated in V2G mode, contributing to a mitigation in system loss induced by EVs within the RDN. This analysis underscores the significance of optimal placement and operation strategies for EVCS, SDG, and DSVC in effectively managing and mitigating power losses in the RDN. The combination of RES and smart compensating devices is critical in improving overall network efficiency and sustainability, even in the presence of dynamic elements such as EV charging operations.

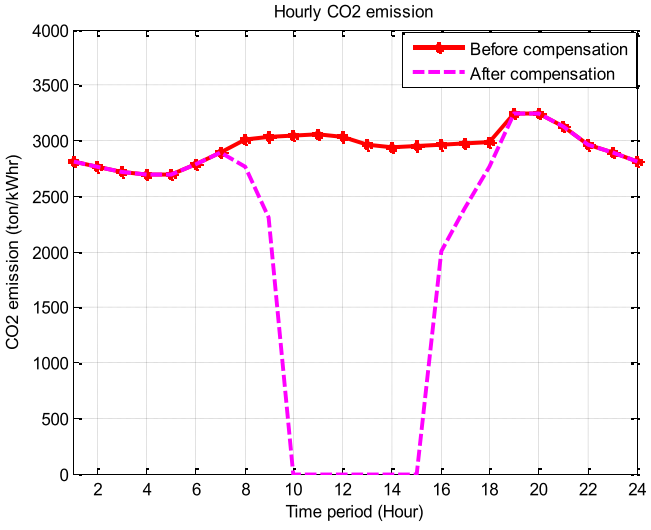

Fig. 18. Hourly CO_2 emission.

4.2.5. Effect of EVCS load on emission

Electricity generation accounts for around 40% of global CO_2 emissions, mostly from the combustion of fossil fuels to generate heat for powering steam turbines. The resulting CO_2 emissions contribute significantly to global warming. Hence, reducing CO_2 emissions is crucial for promoting a sustainable environment. Smart electric grid technologies have the potential to play a pivotal role in achieving such reductions. The effect of EVCS loads on the CO_2 emissions of the RDN was analyzed over a 24-h period, as outlined in Table 4. The results of this analysis are presented below. Fig. 18 visually depicts the hourly CO_2 emissions of the proposed approach. The reduction in CO_2 emissions is achieved by supplying power through SDG and EVCS in V2G mode to the grid. This reduction is particularly notable during the time period from 7 a.m to 7 p.m. The application of SMG technologies, such as integrating renewable energy sources and optimizing the use of EVs in V2G mode, contributes to the reduction of CO_2 emissions.

Furthermore, when the real power is fully supplied to the SMGs by the SDG and EVCS in V2G mode, emissions are nearly eliminated. This observation is evident from Fig. 18, where emissions are close to zero during the hour 10–15, coinciding with the period when SDG and EVCS produce maximum power to the SMGs. It's important to note that SDG alone is not the sole contributor to emission reduction. EVCS in V2G mode also plays a significant role in reducing emissions within the RDN. Additionally, there's a small contribution from BESS when discharging power to the SMGs during peak hours, further aiding in emission reduction efforts. By strategically utilizing clean energy sources and leveraging the capabilities of EVs, the proposed approach aligns with the imperative of mitigating the environmental impact associated with electricity generation. This underscores the potential of smart grid technologies in fostering a more sustainable and eco-friendly energy landscape.

4.3. Comparative analysis

The effectiveness of the IBESA strategy was evaluated using the standardized IEEE 33-test system, with the objective of minimizing the SCOPE index. A thorough assessment was carried out, comparing the performance of well-known algorithms such as Cuckoo Search Algorithm (CSA) (Yang and Deb, 2010), Particle Swarm Optimization (PSO) (Kennedy and Eberhart, 1995), and Genetic Algorithm (GA) (Holland, 1992) against IBESA, all executed under the same conditions. To facilitate comparison, the distribution system load was kept constant at a load factor of 1.0. The optimized results obtained from each optimization method were compiled in Table 5, illustrating a consistent trend that positioned IBESA as the superior approach for minimizing the SCOPE index across all investigated scenarios. Pictorial comparisons of each SCOPE index among the considered optimization methods, including the proposed IBESA, are presented in Figs. 19–23.

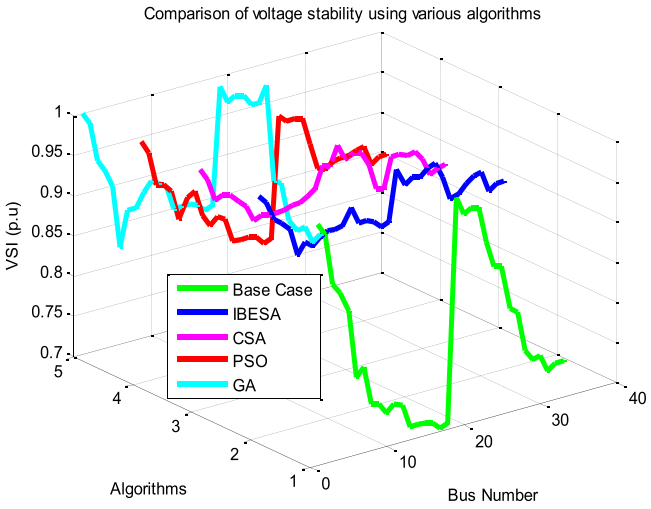

Fig. 19. Comparison of voltage stability profile using various algorithms.

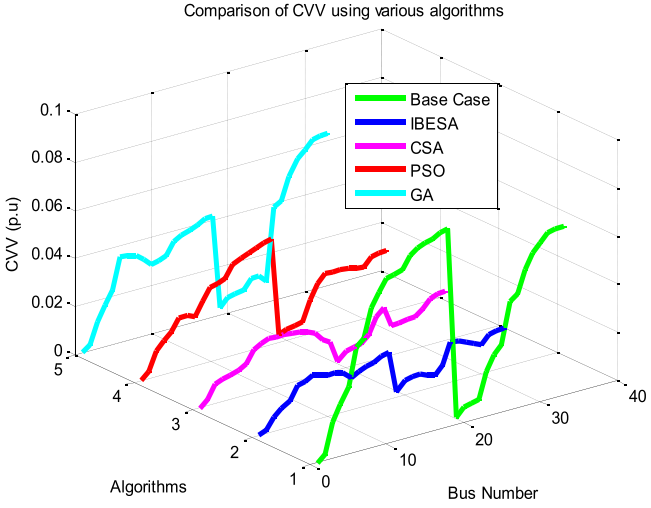

Fig. 20. Comparison of CVV profile using various algorithms.

Fig. 19 illustrates the first index of SCOPE, specifically the stability comparison of several algorithms. It compares the VSI values of each

Table 5
Comparative analysis of results under various optimization algorithms (Constant load).

Parameters	Base Case	IBESA	CSA (Yang and Deb, 2010)	PSO (Kennedy and Eberhart, 1995)	GA (Holland, 1992)
SDG Size in kW (Location)	–	630 (13)	810 (6)	840 (8)	760 (10)
		870 (24)	470 (18)	125 (20)	100 (19)
		920 (30)	690 (29)	750 (30)	730 (25)
DSVC Size in kVAr (Location)	–	310 (13)	450 (6)	420 (8)	540 (10)
		445 (24)	110 (18)	125 (20)	150 (19)
		675 (30)	580 (29)	650 (30)	430 (25)
EVCS Size in kW (Location)	–	325 (2)	1490 (2)	1220 (2)	585 (2)
		405 (19)	440 (19)	420 (19)	190 (19)
		570 (26)	390 (26)	720 (26)	1200 (26)
Stability (p.u)	0.7037	0.9143	0.9119	0.8308	0.7614
CVV (p.u)	0.0823	0.0195	0.0209	0.0437	0.0632
TOC ($)	–	25861.6	27303.5	26603.4	26856.7
Power Loss (kW)	157.56	27.89	38.37	63.34	107.93
Emission (ton/kWhr)	3251	1048.2	1458.3	1690.4	1804.1
Objective Function Value	–	65.06	68.71	67.04	67.76
Convergence time (s)	–	9.89	11.54	13.05	15.09

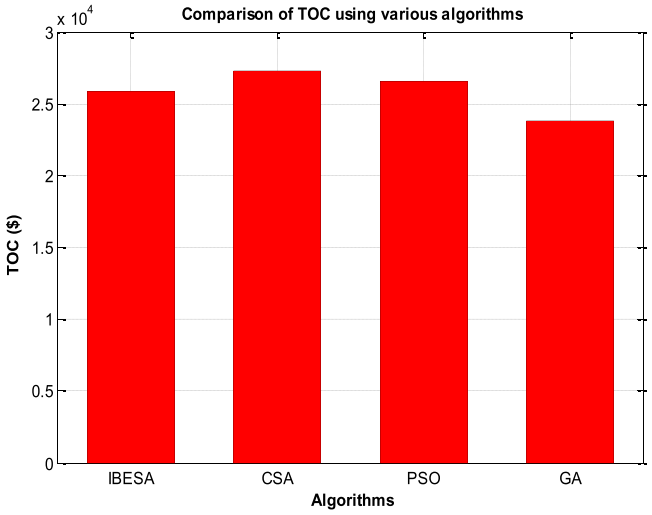

Fig. 21. Comparison of TOC using various algorithms.

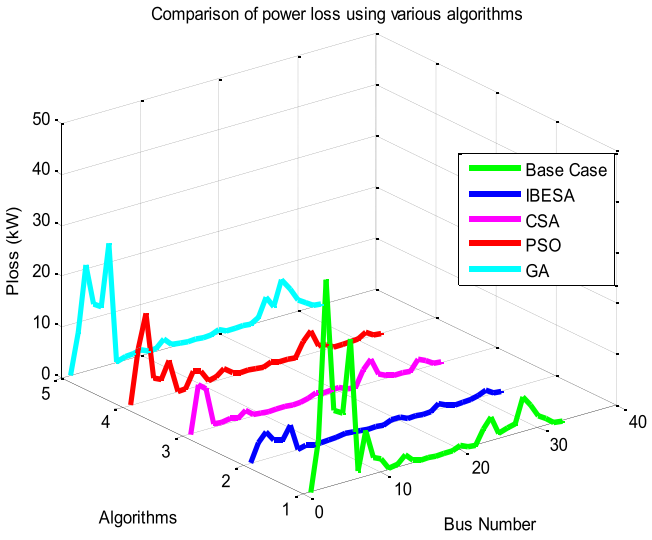

Fig. 22. Comparison of power loss profile using various algorithms.

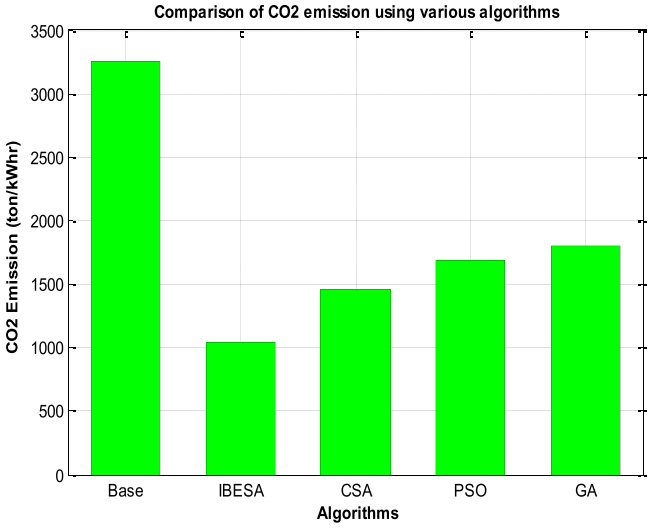

Fig. 23. Comparison of CO_2 emission using various algorithms.

node for both the base case and the optimized case using various algorithms. As indicated in Table 5 and Fig. 19, IBESA consistently produced superior VSI values (IBESA - 0.9143p.u, CSA - 0.9119p.u, PSO - 0.8308p.u, and GA - 0.7614p.u). The second index, CVV, is compared across various algorithms in Fig. 20. By examining the figure and Table 5, it is evident that the proposed IBESA offers better CVV minimization (IBESA - 0.0195p.u, CSA - 0.0209p.u, PSO - 0.0437p.u, and GA - 0.0632p.u). The third index, TOC, is calculated based on SDG, DSVCS, and EVCS sizes, as well as power losses. The bar chart in Fig. 21 highlights the superiority of IBESA in TOC minimization compared to other algorithms (IBESA - 25861.6$, CSA - 27303.5$, PSO - 26603.4$, and GA - 26856.7$). Next, the index of power loss is compared at each node across all algorithms in Fig. 22. Notably, IBESA outperformed competing algorithms such as CSA (38.37 kW), PSO (63.34 kW), and GA (107.93 kW) with a power loss of 27.89 kW. As reported in Table 5 and illustrated in Fig. 22, IBESA displayed more efficient loss reduction. The final index, CO_2 emission reduction, is compared in Fig. 23's bar chart. The suggested IBESA outperformed competing methods in terms of CO_2 emission reduction (IBESA - 1048.2ton/kWhr, CSA - 1458.3ton/kWhr, PSO - 1690.4ton/kWhr, and GA - 1804.1ton/kWhr). This result underscores IBESA's reputation as an innovative solution for effectively minimizing the SCOPE index in the RDN. Based on the above discussion, these findings demonstrate IBESA's potential to address complicated power system difficulties.

The efficacy of an algorithm in attaining the optimal solution is significantly influenced by its reliability in convergence. Fig. 24 illustrates the convergence patterns of various renowned algorithms like CSA, PSO, and GA, as applied to the IEEE 33-bus test system for the MOF. Additionally, Table 5 provides insight into the convergence time for each algorithm. This study lays the groundwork for comprehending the performance of the IBESA algorithm. Notably, IBESA surpasses its competitors in terms of speed, achieving convergence to the optimal objective value within just eight iterations. The distinguishing feature of IBESA lies in its high convergence rate, blending stability, speed, and an exceptional ability for near-global exploration in solving the SCOPE index. When juxtaposed with other algorithms under scrutiny, IBESA stands out for its swiftness and precision in convergence, consistently maintaining a rapid pace of convergence.

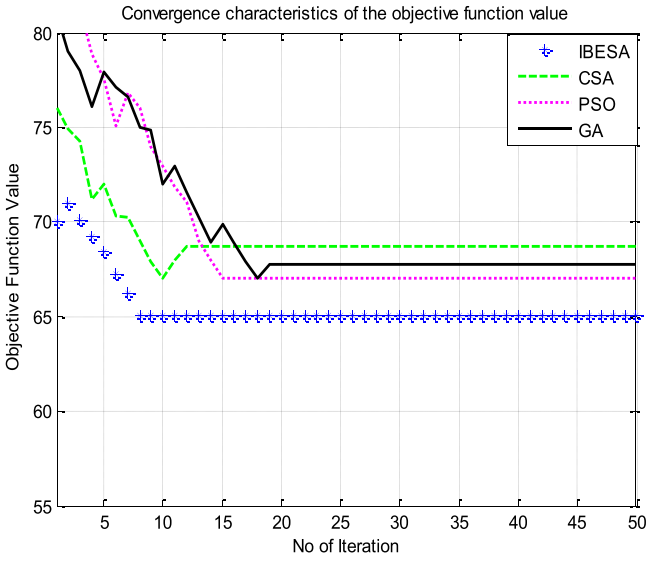

Fig. 24. Comparison of various algorithms convergence characteristics of the objective function value.

4.4. Outcome of SCOPE index

EVs offer environmental benefits by reducing local emissions; however, their integration into the electricity distribution network introduces challenges. This work conducted a comprehensive analysis of the impact of EVCS loads on various technical and economic parameters in the context of the modified IEEE 33-bus RDN. The key findings and observations are summarized below:

- The modified IEEE 33-bus test system demonstrated resilience in accommodating the placement of three EVCSs, SDGs, and DSVCs within SMGs. Beyond three installations, no further reduction in the SCOPE index was observed, indicating the need for network upgrades for additional EVCSs/SDGs/DSVCs.
- Improper placement of EVCSs/SDGs/DSVCs in SMGs adversely affected the SCOPE index, emphasizing the importance of strategic deployment for optimal performance.
- The maximum reduction in the SCOPE index was achieved when SDG units produced the maximum output power, underscoring the significance of RES in improving system performance.
- The SCOPE index, by considering voltage stability, voltage, cost, power loss, and emissions collectively, demonstrated its novelty and efficacy as a comprehensive performance metric.
- The analysis of CO_2 reduction revealed that SDG and EVCS (in V2G mode) contributed significantly to lowering emissions during specific hours.
- The unique aspect of the SCOPE index lies in its ability to simultaneously encompass voltage stability, voltage levels, cost, power loss, and emissions within a unified framework. Additionally, this study introduced a strategy for EVCS placement in SMG based on the IBESA. The outcomes of the optimal EVCS placement, guided by the SCOPE index, affirm the effectiveness and utility of this comprehensive metric in evaluating and optimizing the performance of the distribution network.

4.5. Future direction

Future research directions in this area include:

- **Grid Resilience Strategies:** Explore strategies to enhance grid resilience against potential disruptions caused by the integration of EVCS through advanced control and protective mechanisms.
- **Demand Response Optimization:** Investigate how demand response programs and advanced optimization techniques can be applied to coordinate and optimize the charging and discharging patterns of EVs within the Smart Microgrid, considering both economic and grid stability objectives.
- **Cybersecurity in Smart Grids:** Address the evolving cybersecurity challenges associated with the integration of EVCS and SMGs, ensuring the security and integrity of data and communication networks.
- **Dynamic Pricing Models:** Develop and evaluate dynamic pricing models that encourage users to adopt smart charging behaviors, considering time-of-use pricing and incentives to promote load balancing and grid reliability.
- **Integration of Energy Storage:** Explore the integration of advanced energy storage systems, such as advanced batteries, to mitigate the variability of renewable energy sources and enhance the overall reliability and resilience of the SMG.
- **Advanced Forecasting Techniques:** Develop and implement advanced forecasting techniques for predicting EV charging patterns, renewable energy generation, and overall energy demand within the Smart Microgrid, aiding in better decision-making and resource allocation.
- **Interoperability Standards:** Investigate and establish interoperability standards for seamless integration and communication among different components within the Smart Microgrid, promoting a standardized and efficient system.

These future research directions aim to address emerging challenges and opportunities in the context of SMGs and the integration of EVs, contributing to the advancement and sustainability of smart grid technologies.

5. Conclusions

The rapid global surge in EV adoption, fueled by factors such as low CO_2 emissions, simplified maintenance, and minimal operating costs, prompted extensive research in EVCS. The integration of EVCS into existing distribution grids posed challenges related to potential power losses and voltage variations exceeding acceptable limits. This complexity was exacerbated by the growing prevalence of randomly dispersed solar-based DG and BESS. In response to these challenges, DSVC systems were introduced, offering benefits such as enhanced power transfer capacity and improved voltage regulation without extensive infrastructure upgrades. This research presented the SCOPE framework, encompassing objectives such as minimizing real power loss, reducing bus voltage variation, maximizing system voltage stability, minimizing system operating costs, and mitigating CO_2 emissions indices. The framework leveraged the IBESA to optimize the EVCS placement problem within this multi-objective context. The model accounted for V2G capabilities and user driving patterns over a 24-h horizon. The proposed SMG structure, based on the modification of the standard IEEE 33-bus test RDN, included three interconnected SMGs serving residential, commercial, and industrial users. The ideal position and size of EVCS and RESs were determined using the IBESA-based optimization technique. Results demonstrated the efficacy of integrating SDGs and DSVCs in reducing the SCOPE index, affirming the benefits of the proposed IBESA algorithm. This research provided a comprehensive solution to the intricate challenges associated with EVCS integration, offering a sustainable and optimized approach for future smart microgrids. The success of this study opens avenues for further exploration and implementation of advanced smart grid technologies to foster a cleaner and more efficient energy landscape.

CRediT authorship contribution statement

Sudhakar Babu Thanikanti: Writing – review & editing, Supervision, Resources, Project administration, Investigation. **Nnamdi Nwulu:** Writing – review & editing, Validation, Supervision, Funding acquisition. **Monica P Suresh:** Writing – original draft, Formal analysis, Data curation, Conceptualization. **Yuvaraj T:** Writing – review & editing, Visualization, Software, Resources, Methodology, Investigation.

Declaration of Competing Interest

The authors declare that there is no known competing financial interests or personal relationships that could have appeared to influence the work reported in this paper.

Data Availability

No data was used for the research described in the article.

References

Abou El-Ela, A.A., El-Sehiemy, R.A., Shaheen, A.M., Eissa, I.A., 2020. Optimal coordination of static VAR compensators, fixed capacitors, and distributed energy resources in Egyptian distribution networks. Int. Trans. Electr. Energy Syst. 30 (11), e12609.

Ahmad, F., Bilal, M., 2023. Allocation of plug-in electric vehicle charging station with integrated solar powered distributed generation using an adaptive particle swarm optimization. Electr. Eng. 1–14.

Alanazi, F., 2023. Electric vehicles: benefits, challenges, and potential solutions for widespread adaptation. Appl. Sci. 13 (10), 6016.
Alsattar, H.A., Zaidan, A.A., Zaidan, B.B., 2020. Novel meta-heuristic bald eagle search optimisation algorithm. Artif. Intell. Rev. *53*, 2237–2264.
Amini, M.H.; Boroojeni, K.G.; Wang, C.J.; Nejadpak, A.; Iyengar, S.S.; Karabasoglu, O. Effect of electric vehicle parking lots' charging demand as dispatchable loads on power systems loss. In Proceedings of the 2016 IEEE International Conference on Electro Information Technology (EIT), Grand Forks, ND, USA, 19–21 May 2016; pp. 499–503.
Arif, S.M., Lie, T.T., Seet, B.C., Ayyadi, S., Jensen, K., 2021. Review of electric vehicle technologies, charging methods, standards and optimization techniques. Electronics 10 (16), 1910.
Augugliaro, A., Dusonchet, L., Favuzza, S., Ippolito, M.G., Sanseverino, E.R., 2010. A backward sweep method for power flow solution in distribution networks. Int. J. Electr. Power Energy Syst. 32 (4), 271–280.
Bilal, M., Rizwan, M., 2021. Integration of electric vehicle charging stations and capacitors in distribution systems with vehicle-to-grid facility. Energy Sources, Part A: Recovery, Util., Environ. Eff. 1–30.
Bilal, M., Rizwan, M., 2023. Intelligent algorithm-based efficient planning of electric vehicle charging station: a case study of metropolitan city of India. Sci. Iran. 30 (2), 559–576.
BloombergNEF. New Energy Outlook 2021. Accessed: Aug. 6, 2021. [Online]. Available: ⟨https://about.bnef.com/new-energy-outlook/⟩.
Canizes, B., Soares, J., Costa, A., Pinto, T., Lezama, F., Novais, P., Vale, Z., 2019. Electric vehicles' user charging behaviour simulator for a smart city. Energies 12 (8), 1–20.
Chen, H., Nie, J., Ye, B., 2019. PSO-based siting and sizing of electric vehicle charging stations (November). In: Journal of Physics: Conference Series, vol. 1346. IOP Publishing, 012022 (November).
Chhabra, A., Hussien, A.G., Hashim, F.A., 2023. Improved bald eagle search algorithm for global optimization and feature selection. Alex. Eng. J. *68*, 141–180.
Ćalasan, M., Konjić, T., Kecojević, K., Nikitović, L., 2020. Optimal allocation of static var compensators in electric power systems. Energies *13* (12), 3219.
Darabi, Z., Ferdowsi, M., 2012. Impact of plug-in hybrid electric vehicles on electricity demand profile. Smart Power Grids *2011*, 319–349.
Daramola, A.S., Ahmadi, S.E., Marzband, M., Ikpehai, A., 2023. A cost-effective and ecological stochastic optimization for integration of distributed energy resources in energy networks considering vehicle-to-grid and combined heat and power technologies. J. Energy Storage 57, 106203.
Deb, S., Kalita, K., Gao, X.Z., Tammi, K., & Mahanta, P. (2017, November). Optimal placement of charging stations using CSO-TLBO algorithm. In *2017 Third International Conference on Research in Computational Intelligence and Communication Networks (ICRCICN)* (pp. 84-89). IEEE.
Etezadi-Amoli, M., Choma, K., Stefani, J., 2010. Rapid-charge electricvehicle stations (Jul.). IEEE Trans. Power Del. 25 (3), 1883–1887 (Jul.).
Fazelpour, F., Vafaeipour, M., Rahbari, O., Rosen, M.A., 2014. Intelligent optimization to integrate a plug-in hybrid electric vehicle smart parking lot with renewable energy resources and enhance grid characteristics. Energy Convers. Manag 77, 250–261.
Frade, I., Ribeiro, A., Goncalves, G., & Antunes, A.P. (2010). An optimization model for locating electric vehicle charging stations in central urban areas. Compendium of Papers DVD of TRB 90th Annual Meeting. *Transportation Research Board*.
Gazijahani, F.S., Salehi, J., 2018a. Reliability constrained two-stage optimization of multiple renewable-based microgrids incorporating critical energy peak pricing demand response program using robust optimization approach. Energy 161, 999–1015.
Gazijahani, F.S., Salehi, J., 2018b. Robust design of microgrids with reconfigurable topology under severe uncertainty. IEEE Trans. Sustain. Energy 9 (2), 559–569.
Geleta, D.K., Manshahia, M.S., Vasant, P., Banik, A., 2022. Grey wolf optimizer for optimal sizing of hybrid wind and solar renewable energy system. Comput. Intell. *38* (3), 1133–1162.
Ge, S., Feng, L., & Liu, H. (2011, September). The planning of electric vehicle charging station based on grid partition method. In *2011 International Conference on Electrical and Control Engineering* (pp. 2726-2730). IEEE.
Hanabusa, H., & Horiguchi, R. (2011). A study of the analytical method for the location planning of charging stations for electric vehicles. In *Knowledge-Based and Intelligent Information and Engineering Systems: 15th International Conference, KES 2011, Kaiserslautern, Germany, September 12-14, 2011, Proceedings, Part III 15* (pp. 596-605). Springer Berlin Heidelberg.
Holland, J.H., 1992. Genetic algorithms. Sci. Am. 267 (1), 66–73.
Hung, D.Q., Mithulananthan, N., Lee, K.Y., 2014. Determining PV penetration for distribution systems with time-varying load models. IEEE Trans. Power Syst. *29* (6), 3048–3057.
Jabari, F., Sohrabi, F., Pourghasem, P., Mohammadi-Ivatloo, B., 2020. Backward-forward sweep based power flow algorithm in distribution systems. Optim. Power Syst. Probl.: Methods, Algorithms MATLAB Codes 365–382.
Jamian, J.J., Mustafa, M.W., Mokhlis, H., Baharudin, M.A., 2014. Minimization of power losses in distribution system via sequential placement of distributed generation and charging station. Arab. J. Sci. Eng. *39*, 3023–3031.
Jaramillo, P., Samaras, C., Wakeley, H., Meisterling, K., 2009. Greenhouse gas implications of using coal for transportation: life cycle assessment of coal-to-liquids, plug-in hybrids, and hydrogen pathways. Energy Policy *37* (7), 2689–2695.
Jia, L., Hu, Z., Song, Y., & Luo, Z. (2012, March). Optimal siting and sizing of electric vehicle charging stations. In *2012 IEEE International Electric Vehicle Conference* (pp. 1-6). IEEE.
Kaliaperumal Rukmani, D., Thangaraj, Y., Subramaniam, U., Ramachandran, S., Madurai Elavarasan, R., Das, N., Imran Abdul Rasheed, M., 2020. A new approach to optimal location and sizing of DSTATCOM in radial distribution networks using bio-inspired cuckoo search algorithm. Energies 13 (18), 4615.
Kamruzzaman, M., & Benidris, M. (2018, August). Modeling of electric vehicles as movable loads in composite system reliability assessment. In *2018 IEEE Power & Energy Society General Meeting (PESGM)* (pp. 1-5). IEEE.
Kennedy, J., & Eberhart, R. (1995, November). Particle swarm optimization. In Proceedings of ICNN'95-international conference on neural networks (Vol. 4, pp. 1942-1948). IEEE.
Khalid, M., 2020. Discussion on 'short-term reactive power planning to minimize cost of energy losses considering PV systems'. IEEE Trans. Smart Grid 11, 1812.
Krauter, S., 2018. Simple and effective methods to match photovoltaic power generation to the grid load profile for a PV based energy system. Sol. Energy 159, 768–776.
Liu, Z., Wen, F., Ledwich, G., 2012a. Optimal planning of electric-vehicle charging stations in distribution systems. IEEE Trans. Power Deliv. *28* (1), 102–110.
Liu, Z.F., Zhang, W., Ji, X., & Li, K. (2012b, May). Optimal planning of charging station for electric vehicle based on particle swarm optimization. In *IEEE PES Innovative Smart Grid Technologies* (pp. 1-5). IEEE.
Li, Y., Li, L., Yong, J., Yao, Y., & Li, Z. (2011). Layout planning of electrical vehicle charging stations based on genetic algorithm. In Electrical Power Systems and Computers: Selected Papers from the 2011 International Conference on Electric and Electronics (EEIC 2011) in Nanchang, China on June 20–22, 2011, *Volume 3* (pp. 661-668). Springer Berlin Heidelberg.
Mohamed, A., Salehi, V., Ma, T., Mohammed, O., 2013. Real-time energy management algorithm for plug-in hybrid electric vehicle charging parks involving sustainable energy. IEEE Trans. Sustain. Energy 5 (2), 577–586.
Mohanty, A.K., Babu, P.S., 2021. Optimal placement of electric vehicle charging stations using JAYA algorithm. Recent Advances in Power Systems: Select Proceedings of EPREC 2020. Springer, Singapore, pp. 259–266.
Mozafar, M.R., Amini, M.H., Moradi, M.H., 2018. Innovative appraisement of smart grid operation considering large-scale integration of electric vehicles enabling V2G and G2V systems. Electr. Power Syst. Res. 154, 245–256.
Mu, Y., Wu, J., Jenkins, N., Jia, H., Wang, C., 2014. A spatial–temporal model for grid impact analysis of plug-in electric vehicles. Appl. Energy *114*, 456–465.
Pal, A., Bhattacharya, A., & Chakraborty, A.K. (2019, December). Allocation of EV fast charging station with V2G facility in distribution network. In 2019 8th International conference on power systems (ICPS) (pp. 1-6). IEEE.
Pal, A., Bhattacharya, A., Chakraborty, A.K., 2021. Allocation of electric vehicle charging station considering uncertainties. Sustain. Energy, Grids Netw. 25, 100422.
Phonrattanasak, P., Leeprechanon, N., 2012. Optimal location of fast charging station on residentialdistribution grid. Int. J. Innov., Manag. Technol. *3* (6), 675.
Rakočević, S., Ćalasan, M., Abdel Aleem, S.H.E., 2021. Smart and coordinated allocation of static VAR compensators, shunt capacitors and distributed generators in power systems toward power loss minimization. Energy Sources Part A: Recovery, Util., Environ. Eff. 1–19.
Sadeghi-Barzani, P., Rajabi-Ghahnavieh, A., Kazemi-Karegar, H., 2014. Optimal fast charging station placing and sizing. Appl. Energy *125*, 289–299.
San Román, T.G., Momber, I., Abbad, M.R., Miralles, Á.S., 2011. Regulatory framework and business models for charging plug-in electric vehicles: Infrastructure, agents, and commercial relationships. Energy Policy *39* (10), 6360–6375.
Shaaban, M.F., Mohamed, S., Ismail, M., Qaraqe, K.A., Serpedin, E., 2019. Joint planning of smart EV charging stations and DGs in eco-friendly remote hybrid microgrids (Sep.). IEEE Trans. Smart Grid vol. 10 (5), 5819–5830 (Sep.).
Shaheen, A.M., Elsayed, A.M., Ginidi, A.R., Elattar, E.E., El-Sehiemy, R.A., 2021. Effective automation of distribution systems with joint integration of DGs/SVCs considering reconfiguration capability by jellyfish search algorithm. IEEE Access *9*, 92053–92069.
Shamshirband, M., Salehi, J., Gazijahani, F.S., 2019. Look-ahead risk-averse power scheduling of heterogeneous electric vehicles aggregations enabling V2G and G2V systems based on information gap decision theory. Electr. Power Syst. Res. 173, 56–70.
Simorgh, H., Doagou-Mojarrad, H., Razmi, H., Gharehpetian, G.B., 2018. Cost-based optimal siting and sizing of electric vehicle charging stations considering demand response programmes. IET Gener., Transm. Distrib. *12* (8), 1712–1720.
Sovacool, B.K., Hirsh, R.F., 2009. Beyond batteries: an examination of the benefits and barriers to plug-in hybrid electric vehicles (PHEVs) and a vehicle-to-grid (V2G) transition. Energy Policy 37 (3), 1095–1103.
Sriabisha, R., & Yuvaraj, T. (2023, March). Optimum placement of Electric Vehicle Charging Station using Particle Swarm Optimization Algorithm. In 2023 9th International Conference on Electrical Energy Systems (ICEES) (pp. 283-288). IEEE.
Teng, J.H., Luan, S.W., Lee, D.J., Huang, Y.Q., 2012. Optimal charging/discharging scheduling of battery storage systems for distribution systems interconnected with sizeable PV generation systems. IEEE Trans. Power Syst. *28* (2), 1425–1433.
Thangaraj, Y., Kuppan, R., 2017. Multi-objective simultaneous placement of DG and DSTATCOM using novel lightning search algorithm. J. Appl. Res. Technol. *15* (5), 477–491.
Tran-Quoc, T., Le Pivert, X., Saheli, M., & Beaude, O. (2012, October). Stochastic approach to assess impacts of electric vehicles on the distribution network. In 2012 3rd IEEE PES Innovative Smart Grid Technologies Europe (ISGT Europe) (pp. 1-8). IEEE.
Wang, G., Xu, Z., Wen, F., Wong, K.P., 2013. Traffic-constrained multiobjective planning of electric-vehicle charging stations. IEEE Trans. Power Deliv. *28* (4), 2363–2372.

Yang, X.S., Deb, S., 2010. Engineering optimisation by cuckoo search. Int. J. Math. Model. Numer. Optim. 1 (4), 330–343.
Yuvaraj, T., Devabalaji, K.R., Thanikanti, S.B., Aljafari, B., Nwulu, N., 2023a. Minimizing the electric vehicle charging stations impact in the distribution networks by simultaneous allocation of DG and DSTATCOM with considering uncertainty in load. Energy Rep. 10, 1796–1817.
Yuvaraj, T., Devabalaji, K.R., Thanikanti, S.B., Pamshetti, V.B., & Nwulu, N. (2023b). Integration of Electric Vehicle Charging Stations and DSTATCOM in Practical Indian Distribution Systems using Bald Eagle Search Algorithm. IEEE Access.
Yuvaraj, T.K.R.D., Devabalaji, K.R., Thanikanti, S.B., 2020. Simultaneous allocation of DG and DSTATCOM using whale optimization algorithm. Iran. J. Sci. Technol., Trans. Electr. Eng. 44, 879–896.
Yuvaraj, T., Suresh, T.D., Ananthi Christy, A., Babu, T.S., Nastasi, B., 2023a. Modelling and Allocation of Hydrogen-Fuel-Cell-Based Distributed Generation to Mitigate Electric Vehicle Charging Station Impact and Reliability Analysis on Electrical Distribution Systems. Energies 16 (19), 6869.
Yuvaraj, T., Suresh, T.D., Meyyappan, U., Aljafari, B., & Thanikanti, S.B. (2023c). Optimizing the allocation of renewable DGs, DSTATCOM, and BESS to mitigate the impact of electric vehicle charging stations on radial distribution systems. Heliyon.